The periplasmic space cannot be artificially enlarged due to homeostatic regulation maintaining spatial constraints essential for membrane spanning processes and cell viability.

Eric Mandela[1,+], Christopher J. Stubenrauch[1,+], David Ryoo[2], Hyea Hwang[3,#], Eli J. Cohen[4], Von L. Torres[1], Pankaj Deo[1], Chaille T. Webb[1], Cheng Huang[5], Ralf B. Schittenhelm[5], Morgan Beeby[4], JC Gumbart[6,*], Trevor Lithgow[1,*] & Iain D. Hay[7,*]

1 - Infection & Immunity Program, Biomedicine Discovery Institute and Department of Microbiology, Monash University, Clayton, 3800, Australia

2 - Interdisciplinary Bioengineering Graduate Program, Georgia Institute of Technology, Atlanta, GA 30332, USA

3 - School of Materials Science and Engineering, Georgia Institute of Technology, Atlanta, Georgia 30332-0430, USA

4 - Department of Life Sciences, Imperial College London, London SW7 2AZ, UK.

5 - Monash Proteomics & Metabolomics Facility, Department of Biochemistry and Molecular Biology, Biomedicine Discovery Institute, Monash University, Clayton, 3800, Australia

6 - School of Physics, Georgia Institute of Technology, Atlanta, Georgia 30332-0430, USA

7 - School of Biological Sciences, The University of Auckland, Auckland 1010, New Zealand

- Present address: NIH Center for Macromolecular Modeling and Bioinformatics, Beckman Institute for Advanced Science and Technology, Department of Biochemistry, Center for Biophysics and Quantitative Biology, University of Illinois at Urbana-Champaign, Urbana, IL, USA

+ - These authors contributed equally

* - To whom correspondence should be addressed: iain.hay@auckland.ac.nz, trevor.lithgow@monash.edu, jcgumbart@gatech.edu

ABSTRACT

The cell envelope of Gram-negative bacteria consists of two membranes surrounding a periplasm and peptidoglycan layer. Molecular machines spanning the cell envelope dictate protein and lipid transport and drug resistance phenotypes, and depend on spatial constraints across the envelope and load-bearing forces across the cell surface. The mechanisms dictating spatial constraints across the cell envelope remain incompletely defined. In *Escherichia coli*, the coiled-coil lipoprotein Lpp contributes the only covalent linkage between the outer membrane and the underlying peptidoglycan layer. Using proteomics, molecular dynamics and a synthetic lethal screen we show that lengthening Lpp to the upper limit does not change periplasmic width and spatial constraint, but rather impacts the load-bearing capacity across the outer membrane. *E. coli* expressing elongated Lpp activate potent homeostatic mechanisms to enforce a wild-type spatial constraint: they increase steady-state levels of factors determining cell stiffness, decrease membrane integrity, increase membrane vesiculation and depend on otherwise non-essential tethers to maintain lipid transport and peptidoglycan biosynthesis. Our findings demonstrate complex regulatory mechanisms for tight control over periplasmic width to enable spatial constraint essential for membrane spanning processes. They further show that the periplasm cannot be widened by engineering approaches, with implications for understanding how spatial constraint across the envelope controls processes such as flagellum-driven motility, cellular signaling and protein translocation.

INTRODUCTION

Gram-negative bacteria have a cell envelope composed of two membranes sandwiching between them an aqueous space called the periplasm, in which an essential structural layer of peptidoglycan (PG) resides. The outer membrane is critical to cell growth and these bacteria face challenges to their cell biology in terms of membrane protein assembly and lipid-transport pathways that must traverse the distance from the inner membrane (IM) to the outer membrane (OM) [1]. Recent work investigating the spatial demands for assembly of proteins into the outer membrane has shown precincts of active protein integration into the membrane can deliver new material to the growing outer membrane [2] and that random planar movement from these precincts drives the observed non-uniform distributions of the major proteins of the outer membrane [3, 4]. By contrast to these protein components that diffuse to the outer membrane, elements of the lipid-transport machinery (eg. the Lpt complex) [5, 6, 7, 8, 9] span the OM and IM in order to fulfil their function in delivering lipid components to the outer membrane.

The PG layer is a fundamental aspect of the cell envelope, and it must be dynamically remodeled to allow growth as well as the assembly and transit of trans-envelope structures. PG synthesis and remodeling is a complex process with high levels of redundancy at various steps, involving at least 50 enzymes in *E. coli* [10]. The Penicillin-binding proteins (PBPs) are the core components responsible for the periplasmic biosynthesis of peptidoglycan. There are multiple PBP complexes including the two core, semi-redundant PBP complexes PBP1a and PBP1b embedded in the IM which are activated by interactions with lipoproteins LpoA and LpoB embedded in the OM. Thus the activation of PG synthesis by these enzymes is spatially regulated, serving as a self-limiting molecular ruler to modulate PG thickness [11]. Cells must possess either a functional PBP1a or PBP1b system for growth [12, 13].

Trans-envelope complexes such as lipopolysaccharide (LPS) transit pathways [5, 6, 7, 8, 9] and the protein translocation and assembly module (the TAM) [14, 15, 16] are also spatially constrained by the need to reach across from the IM to OM in order to function. The PG layer is covalently attached to the outer membrane by Braun's lipoprotein (Lpp), with two recent papers addressing whether extending the length of Lpp would impact on (i) flagellar function given that the flagellum spans both membranes [17], and (ii) signal-transduction systems that span the OM to IM [18]. In both cases, extending the coiled-coil structure of Lpp by 21 residues (Lpp^{+21}) was found to be the longest form that supported close to normal growth [17, 18]. Imaging of these Lpp^{+21} strains in both studies suggested that the total periplasmic width had been stretched from ~9.5nm to ~11.5nm [17, 18]. This being the case, the Lpp^{+21} model would provide a powerful experimental system to study how processes like OM biogenesis and PG biosynthesis can be maintained under a spatial stress on the cell wall.

To understand how trans-envelope processes in *E. coli* adapt to the presence of an enlarged periplasm, a combination of phenotypic analysis, proteomics, molecular dynamics and a synthetic lethal screen was employed to identify and characterize factors needed to maintain viability in the Lpp^{+21} strain of *E. coli*. The genetic screen demanded synthetic growth phenotypes from an array of mutants each lacking a gene that, while non-essential in wild-type *E. coli* [19], is essential in the Lpp^{+21} strain. These genes fall into three functional categories: PG biosynthesis and remodelling, LPS biosynthesis and PG-outer membrane linkage. We show that previously non-essential proteins involved in bridging the gap between the OM and PG become essential in the context of the Lpp^{+21} strain background. These include previously known PG binding OM proteins (OmpA and Pal) as well as proteins previously not known to play an active role in linking the OM and PG (TolC and YiaD). We observed a thicker more diffuse or heterogeneous PG layer in the Lpp^{+21} strain and whole cell proteomics revealed that in response to an increased length of Lpp, *E. coli* increases the levels of a range of cell envelope proteins involved in PG turnover. We discuss the outcomes in terms of how the PG-outer membrane linkage functionalizes the periplasm, the evolutionary constrains in place to maintain this functionality, and the specific activity of Lpp in contributing to the load-bearing function of the OM.

RESULTS

Resilience and growth of the Lpp^{+21} strain

A phylogenetic assessment of Lpp lengths across diverse bacterial lineages showed a very narrow window of protein size (Fig. 1A), with Lpp being 78 residues in most species of bacteria including *E. coli*. Lpp lengths of 99 residues or more are at the upper end of the natural range for this protein and, in nature, these longer Lpp proteins are found in the genus *Geobacter*. The previously described Lpp^{+21} isoform expressed in *E. coli* therefore sits near the upper limit in the natural range. We introduced a gene encoding the Lpp^{+21} isoform into an *E. coli* background suitable for genetic screens (Fig. S1) and confirmed the size of the protein by SDS-PAGE of bacterial cell extracts (Fig. 1B). Enteric bacteria like *E. coli* have evolved in environments that are not nutrient-rich and are hyper-osmotic with respect to most laboratory growth medium [20, 21]. The Lpp^{+21} isoform had little impact on growth of *E. coli*. On minimal growth medium, growth rates of the Lpp^{+21} strain of *E. coli* were equivalent to the isogenic wild-type *E. coli* (Fig. 1C). This was likewise true on growth media osmotically balanced with concentrations of sorbitol up to 1.0M (Fig. 1D), and on rich (LB) medium with or without sorbitol (Fig. 1D).

To establish the extent to which the periplasm had been remodeled in the Lpp^{+21} strain of *E. coli*, samples were prepared for cryogenic transmission electron microscopy, a technique in which cells are preserved in a frozen-hydrated, near-native state. As expected, the average width of the periplasm was increased in both strains under hyperosmotic conditions when compared to previously reported data where cells were grown in standard laboratory media [18]. As shown in Fig. 1E, the averaged values for the periplasmic width were only slightly greater in the Lpp^{+21} strain (32-36nm) compared to the isogenic wild-type strain (30-32nm). As evident in individual micrographs, the distance to the center of the PG density from the OM was slightly increased in the Lpp^{+21} strain (Fig. 1F). The PG morphology was also changed: in the wild-type strain a uniform dark PG layer could be observed in the images, whereas in the Lpp^{+21} strain a thicker defuse PG layer is present in the images, indicating heterogeneity in both the density and thickness of the PG.

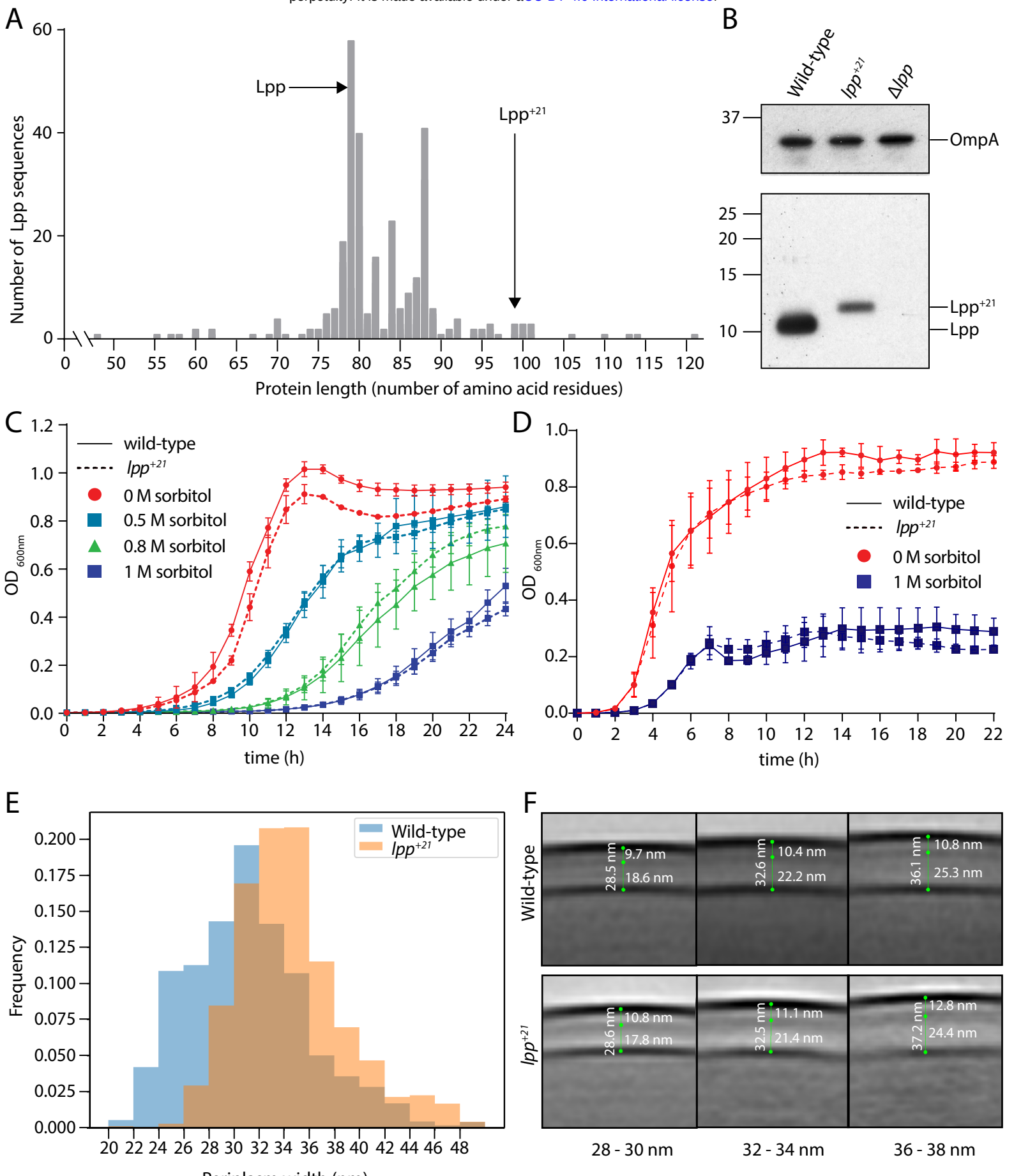

Figure 1. Phenotypes of E. coli cells encoding the Lpp^{+21} isoform. (A) Non-redundant Lpp sequences were identified (Methods) and the protein length charted on the x-axis. The number of non-redundant sequences showing that length is shown on the y-axis. The location of Lpp and the lengthened Lpp^{+21} are indicated. (B) Whole cell lysates were prepared from the indicated strains and subject to SDS-PAGE and immunoblot analysis with anti-Lpp antibodies and anti-OmpA antibodies. OmpA serves as a loading control. (C) The JW5028 – Keio BW25113 strain with kan gene replacing a pseudogene background and isogenic Lpp^{+21} strain (Fig. S1) were grown over 24 hours. The growth medium is M9, containing the indicated concentration of sorbitol as an osmolyte. (D) Growth rates for the same strains were measured in rich (LB) growth media with and without sorbitol over 20 hours. (E) The periplasmic width distribution of the indicated strains in hyperosmotic conditions. While PG layer in the wild-type strain is a uniform thin electron dense layer, the PG layer in the Lpp^{+21} strain is more diffuse and thicker. (F) Cryo EM of cell envelopes in hyperosmotic conditions. Measurements from EM views evaluate the distance between OM and PG in the Lpp^{+21} strain micrographs. The histogram depicts the frequency with which a given distance is observed between the OM and PG.

Homeostasis in the periplasm

To determine the adaptive response to changing the distance constraint between OM and PG, quantitative whole cell proteomics was applied to evaluate the Lpp^{+21} strain. Triplicate samples of the wild-type and Lpp^{+21} strains were processed for analysis by mass spectrometry and we sought to identify those proteins where the steady-state level increases or decreases three-fold or more (Log_2 fold change of ± 1.6) in the Lpp^{+21} strain (Fig. 2A; Table S1). The level of the oligopeptide transporter subunits (OppB, OppC, OppD and OppF) are substantially increased in the Lpp^{+21} strain compared to the wild-type (Table S2). This suggests an increase in PG turnover and an overall increased capacity to recycle PG components, and is consistent with the concomitant increase in AmiC, one of the two major amidases involved in PG remodeling. In addition, proteins implicated in diverse stress-responses (cold shock proteins CspG, CspA, CspI and YdfK, as well as envelope stress protein ZraP and redox stress protein YfcG) were observed at increased steady-state levels in Lpp^{+21} strain (Fig. 2A, Table S2). The greatest decreases were seen in the steady state levels of the GatZABCD proteins involved in galactitol phosphotransferase system and DHAP synthesis (Fig. 2A). The *gatABCD* genes have been shown to be responsive to factors that change *E. coli* cell surface tension [22] and Lpp^{+21} has been reported to significantly decrease cell stiffness [23].

A decrease was seen in the steady-state level of the Lpp^{+21} isoform in the mutant, to approximately one-eighth the level of Lpp in the wild-type strain (Fig. S2). This is consistent with the relative abundance of Lpp and Lpp^{+21} observed in SDS-PAGE analysis of cell extracts from the two strains (Fig. 1F). However, despite the relative decrease, Lpp^{+21} remains as a highly abundant component of the OM-PG linkage factors given that Lpp is present at up to 10^6 protein molecules per wild-type cell [1, 24].

The mass spectrometry data was processed to allow for an analysis of sub-cellular proteomes [25] (Fig S3). An initially puzzling observation was that the Lpp^{+21} strain has a 12% overall reduction of total periplasmic protein compared to wild type (Fig. 2B). This was calculated as the proportion of the summed intensity from identified proteins predicted to reside in the periplasm in the STEPdb: G, E, F2, F3, I annotations [25] (Fig S3). Lpp^{+21} strains of *E. coli* are softer as previously judged by atomic force microscopy [23], and factors that increase the softness of *E. coli* also increase outer membrane vesicle (OMV) production [26]. To address whether the measured depletion of periplasmic content reflects an increased production of OMVs, extracts measuring the amount of total protein in the OMV fraction were normalized to OD_{600} (Fig 2C, Fig. S3). This confirmed that the presence of Lpp^{+21} promotes approximately 10-fold more total protein associated with the OMV fraction, reflecting increased OMV production. The overall level of OM proteins associated with the cells was maintained constant (Fig. S3) but a small OM integrity defect was evident from an increased sensitivity to SDS (Fig. 2D).

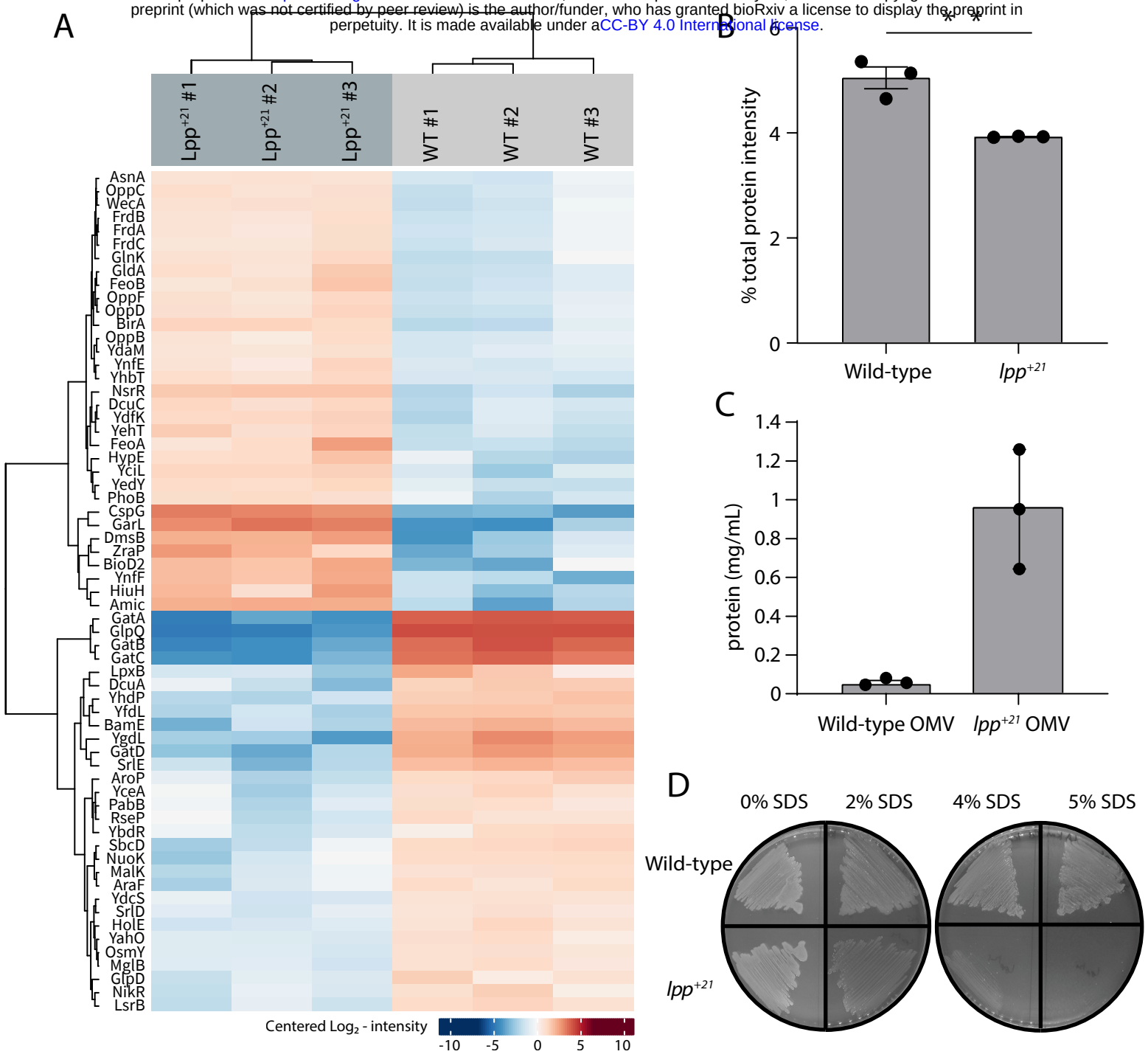

Figure 2. The Lpp+21 cells have softened outer membranes and increased blebbing. (A) Heat map of the significant proteomic differences observed between the wild-type and Lpp^{+21} mutant. Blue boxes indicate a relative reduction and red indicates a relative increase in protein level, centred on the average of the replicate samples. The grouping of the proteins is based on the similarity of the change in expression observed. (B) The Lpp^{+21} mutant has an overall reduction in the level of periplasmic proteins. (C) The Lpp^{+21} mutant has an increase in protein secreted via OMV blebbing. (D) SDS sensitivity profiles of the Lpp^{+21} mutant compared to the wild-type in increasing concentration of SDS in LB (solid) media. Representative data are shown from experiments performed in triplicate.

Lpp^{+21} can be accommodated in the periplasm, but other factors become essential

To directly address the altered phenotype induced by Lpp^{+21}, we established a robotic synthetic genetic array for factors in *E. coli* that become essential in order to maintain viability of the Lpp^{+21} strain (Fig S4). The screen demands synthetic growth phenotypes from an array of mutants each lacking a gene that, while non-essential in wild-type *E. coli*, become essential in the Lpp^{+21} strain of *E. coli*. The endogenous *lpp* gene was replaced by a gene encoding Lpp^{+21} in a isogenic library of 3818 *E. coli* mutants, each of which lacks a non-essential gene. Growth on rich medium allowed the rescue of the new library for array into a format suitable for high-throughput screening with a Singer RoToR robotics platform (Fig S4). Phenotypic analysis was thereafter scored for growth by comparing the growth of the isogenic mutants in the Lpp background (Fig. 3A) with the equivalent mutants in the Lpp^{+21} background (Fig. 3B). Each of the genes that displayed a noticeable phenotype in these analyses are presented in Table 1.

The only cytoplasmic factor identified in our screen, YraN is predicted to be a Holliday-junction resolvase related protein, and we therefore speculate that this mutant failed to resolve the merodiploid condition transient in the introduction of the *lpp*$^{+21}$ condition to the background strain, making the *yraN* mutant a technique-relevant artefact of the screen. This being the case, only functions performed in the periplasm were recovered as essential to viability for the Lpp^{+21} strain.

Most of the components of the LPS biosynthetic machinery are essential genes in *E. coli* and are thus not represented in the library of non-essential genes. Those few, non-essential genes in the LPS biosynthetic pathway that are in the library, become essential to the Lpp^{+21} strain (Table 1): the core LPS biosynthesis factors GalU, GmhB and RfaD were shown to be essential in the Lpp^{+21} strain. The gene encoding the protease YcaL was also detected as essential in the Lpp^{+21} strain, consistent with its proposed function in LPS biogenesis through quality control of LptD function [27].

An essential role for keeping the OM-PG distance

Several genes encoding proteins that could play roles in anchoring the PG within the cell envelope were identified as essential in the Lpp^{+21} background. Independently, none of the major proteins bridging the OM and PG are essential for growth in *E. coli* [19] and all are therefore represented in the library. In a Lpp^{+21} background the genes encoding the β-barrel protein OmpA and the lipoprotein Pal become essential (Table 1). PG-binding domain PF00691 is common to these proteins: appended to a beta-barrel in OmpA, but to a lipoyl anchor in Pal, and is also conserved in other proteins across diverse Gram-negative bacteria (Fig 3C). In *E. coli* there are 4 additional proteins containing this PG-binding domain and these were mapped in a sequence similarity network analysis (Fig 3D). A protein of unknown function, YiaD, is present (Fig 3D) and it too is essential in a Lpp^{+21} background (Table 1). We suggest, therefore, that this protein plays a substantive role in OM-PG linkage. The remaining three proteins: MotB, LafU and YfiB, are more divergent to the

192 OmpA/Pal/YiaD cluster. Neither *motB*, *lafU* nor *yfiB* displayed a synthetic phenotype with Lpp^{+21}, and it has
193 been suggested previously that *motB*, *lafU* and *yfiB* are not expressed at detectable levels under laboratory
194 conditions [28].
195
196 Detecting genes encoding drug-efflux pumps as important for growth of the Lpp^{+21} strain was initially
197 surprising. Either the absence of the inner membrane proteins AcrB or the OM component TolC caused a
198 reduction of growth in the Lpp^{+21} genetic background (Table 1). When antibiotic selection was removed by
199 plating the mutants on medium without chloramphenicol, the synthetic growth defects were observed in the
200 absence of drug selection (Fig. 3D), indicating that this synthetic phenotype is not the result of a decreased
201 drug efflux activity. The trans-envelope AcrAB-TolC multidrug efflux pump has been shown to traverse
202 through the PG and interact directly with PG at several defined sites [29, 30, 31, 32], and we suggest that this system
203 acts as an additional OM-PG linkage that becomes essential in a Lpp^{+21} background. Together with the
204 observation that OmpA, Pal, YiaD and TolC are also essential in the Lpp^{+21} genetic background, these data
205 suggest that functions that maintain local areas of closer contact between the OM and PG are essential for
206 viability.
207

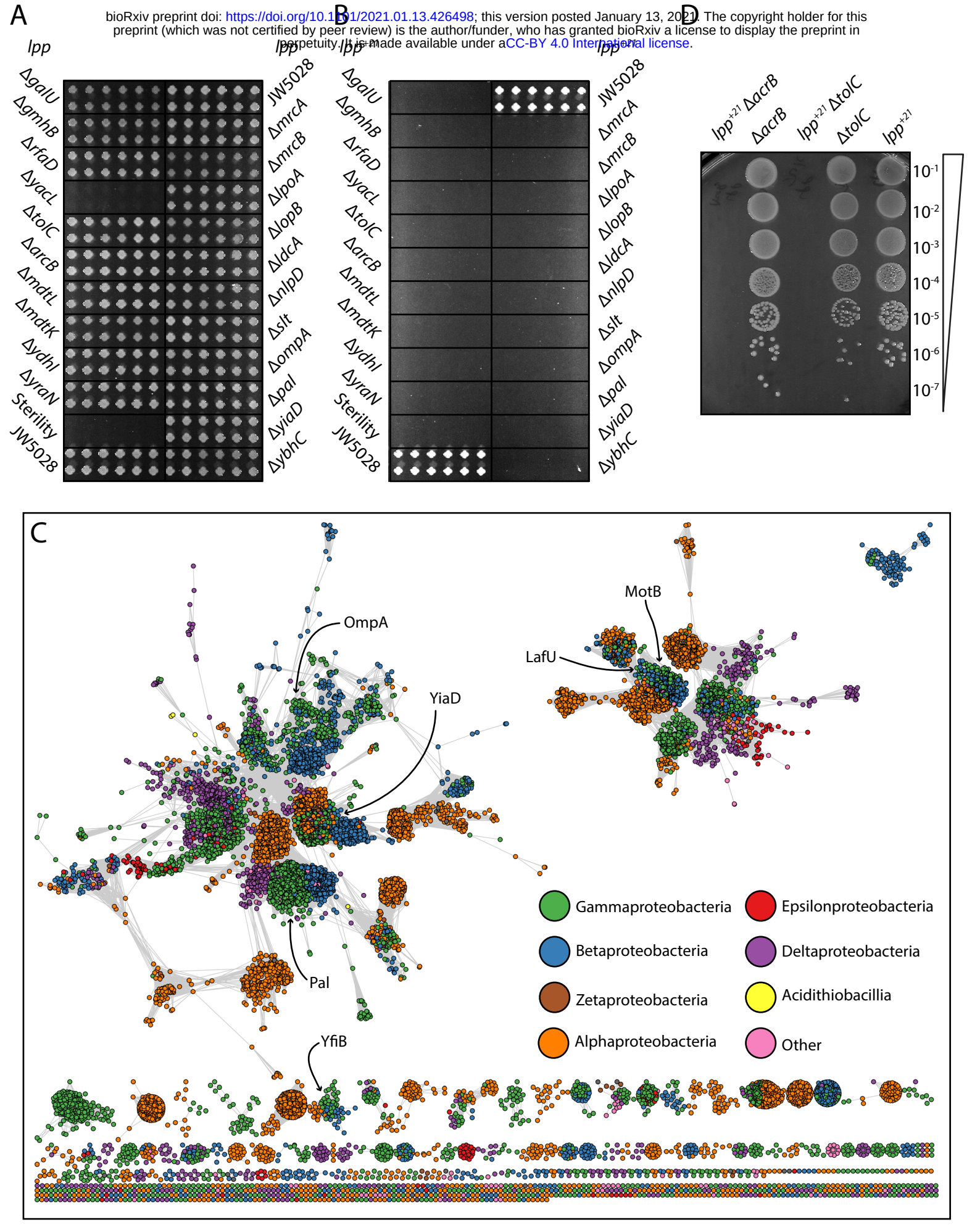

Figure 3. Factors that become essential to mediate OM-PG linkage in Lpp^{+21} E. coli. (A) The growth phenotype in M9 minimal media (0.5 M sorbitol) of single gene knock outs that exhibit essentiality on Lpp^{+21} background (Table 1). (B) The growth phenotype in M9 minimal media (0.5 M sorbitol) of double gene mutants. The mutants are results of Hfr Cavalli lpp:lpp^{+21} cat crossed with 22 KanR recipients shown in panel A (methods). The double mutants are indicated and are arranged in 4 biological replicates (each having 4 technical replicates). (C) Sequence similarity network of domain (Pfam PF00691) containing proteins from across the Proteobacteria. Each circle represents a protein from a representative proteome (rp35) containing the PF00691 domain, connected by lines with a length imparted by their similarity score as defined by EFI - Enzyme Similarity Tool 60, with a cutoff of 30. Proteins are colored by their taxonomic class and the approximate location of the E. coli K12 six PF00691 proteins is indicated. (D) Synthetic lethal phenotype of the drug efflux mutants in the absence of selective antibiotics in M9 minimal media condition. Representative data are shown from experiments performed in biological triplicate.

209 **Table 1. Essential genes in the Lpp^{+21} strain**

210

Cellular process	**Lpp^{+21}-essential genes**	**Function**
LPS biosynthesis	*galU*	UDP-glucose metabolic process
	gmhB/*yaeD*	ADP-L-glycero-β-D-manno-heptose biosynthetic process
	rfaD/*hldD*/*waaD*	ADP-L-glycero-β-D-manno-heptose biosynthetic process
	ycaL	YcaL is a quality-control protease acting on LptD
Peptidoglycan biosynthesis, turnover and remodelling	*lpoA, lpoB,*	Regulators of PG synthases
	mrcA, mrcB	PG synthases
	ldcA	L,D-carboxypeptidase involved in PG recycling/turnover
	nlpD	Regulator of AmiC PG hydrolase
	slt	Lytic PG transglycosylase, degradation of uncrosslinked glycan strands
	ybhC	Carbohydrate esterase, PG turnover
PG-OM linkage	*acrB, mdtL, mdtK, ydhI*	IM components of drug efflux pumps.
	tolC	OM component of drug efflux pump
	ompA	β-barrel protein with PG binding domain
	pal	Lipoprotein with PG binding domain
	yiaD	Lipoprotein with PG binding domain

211

To compare the behaviors of Lpp and Lpp^{+21}, both with and without an OmpA monomer present, molecular dynamics (MD) simulations were run for 200 ns each (see Methods for details). The Lpp lipoprotein from *E. coli* is a triple coiled-coil that would be anchored to the inside face of the outer membrane by its N-terminal acyl group with a length equating to approximately 7.5 nm [33]. The experiments were established to test the scenario for Lpp trimers or Lpp^{+21} trimers in the absence or presence of an OmpA tether between the patch of OM and patch of PG (Fig. 4). For three of the systems: Lpp only, Lpp with OmpA, and Lpp^{+21} only, tilting was marginal, with tilt angles of 83±6°, 82±5°, and 79±3°, respectively (all numbers from the last 100 ns of the 200-ns trajectory). These angles are in agreement with previous simulations of Lpp alone (~80°) and slightly larger than those of Lpp with an OmpA monomer (~75°) PG [34, 35]. In initial simulations of Lpp^{+21} with OmpA, the non-covalent connection between OmpA and PG was quickly disrupted as Lpp^{+21} extended from its kinked state. Therefore, the simulation was repeated with an enforced OmpA-PG connection. Lpp^{+21} was observed to both straighten and tilt within the first 100 ns; the tilt angle measured for the last 100 ns was 70±5°.

The distance between the OM inner leaflet phosphorus atoms and the PG sugars was measured in each scenario. In the presence of Lpp, the distances with and without OmpA were similar at 8.3±2.1 nm and 8.1±1.2 nm, respectively. This was not true for the other scenarios where the distance for Lpp^{+21} alone was 11.6±1.3 nm, but for Lpp^{+21} with OmpA, the distance was reduced significantly to 8.7±2.7 nm. Thus, we observe that PG-binding proteins like OmpA can counteract the increased distance imposed by Lpp^{+21}, inducing it to tilt significantly in accommodation. We also compared our simulations to the distances that were measured by EM (centre of the OM to centre of the PG). In wild-type *E. coli* (i.e. Lpp+OmpA), the centre-centre distance in the simulations is 10.7 +/- 2.2 nm (Fig 4B), similar to the 9.7 -10.8 nm measured in intact cells (Fig. 1F). The centre-centre distance measured in the simulation of Lpp^{+21} tilted by the presence of OmpA (11.0 +/- 2.6 nm), fits the observed distances of 10.8 – 12.8 nm much better than the distance that would be created by a perpendicular Lpp^{+21} (14.2 +/- 1.3 nm).

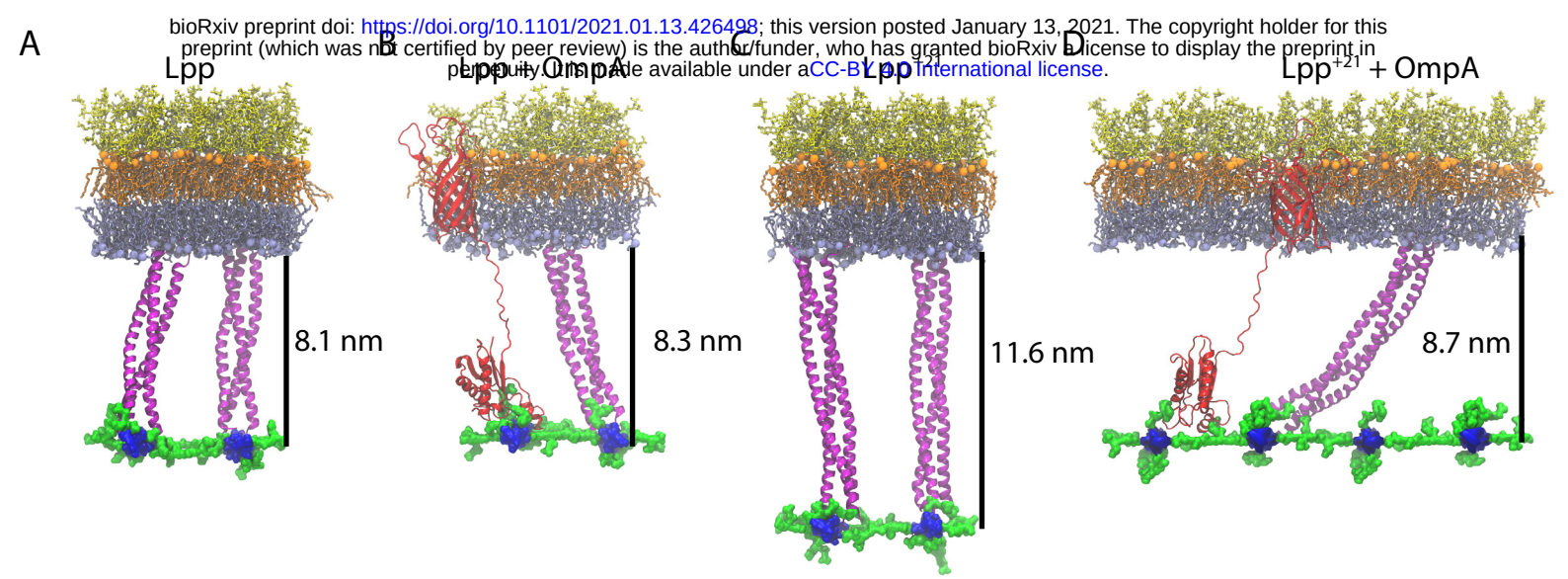

Figure 4

Figure 4. Final states of the OM-PG linkage from MD simulations. (A-B). A patch of OM with the LPS molecules depicted in orange (lipid A moiety) and yellow (core oligosaccharides), and the phospholipids in the inner leaflet of the OM depicted in grey. The PG layer (blue for glycans and green for peptide crosslinks) is attached to the OM via two trimers of Lpp (A), or a trimer of Lpp and the PG-binding domain of OmpA (red). The β-barrel anchor of OmpA is shown embedded in the OM. (C-D) Equivalent scenarios formed with Lpp^{+21} trimers. The distances shown are calculated from the inner face of the OM to the centre of the PG layer and represent the average over the last 100 ns of a 200-ns simulation.

DISCUSSION

We observed that over a range of osmotic conditions, and in nutrient-rich or nutrient-poor media, growth rates of the Lpp^{+21} strain of *E. coli* were equivalent to the isogenic wild-type *E. coli*, suggesting bacteria can adapt to the presence of the extended Lpp^{+21}. We did not observe the uniform 116 % increase to the OM-IM space reported [17, 18, 23] and reviewed [23, 36]. Instead, a range of distances were measured and three adaptive features were expressed as phenotypes in the Lpp^{+21} strain: (i) the steady-state level of the Lpp^{+21} tether was reduced eight-fold compared to the level of Lpp in the isogenic wild-type strain, and other tethers that enforce a wild-type distance: OmpA, Pal, YiaD and TolC, became essential factors in the Lpp^{+21} condition, (ii) structures that depend on a wild-type OM-IM distance, such as the LPS transport system, continued to function but all components of the system became essential for cell viability, and (iii) the PG network took on characteristics of dysregulated synthesis and all components of the otherwise redundant PG biosynthesis pathways become essential to viability.

Tethers that enforce the distance constraint between the OM and PG layer became essential factors in the Lpp^{+21} condition

The lipoyl-N-terminus of Lpp is integrated into the OM, and the C-terminus of a protomer of the Lpp trimer is covalently linked to the PG layer. Stereochemically, only one unit of a Lpp trimer can be covalently attached to the PG layer, and this stoichiometry has been observed experimentally [33, 34, 37]. This makes each Lpp trimer an important bridge between the OM and PG layers of the cell wall, but it has not been clear whether the core role of Lpp is acting in compression or tension. In other words[38], is the role of Lpp to be a supportive brace to keep the OM away from the PG, or a binding anchor to bring the OM as closely as possible to the PG? In a wild-type *E. coli* scenario, molecular dynamics simulations show that the flexible linkers in PG-binding proteins like OmpA allow for adjustments in positioning the PG relative to the OM. In the presence of Lpp, the flexible linker of the PG binding domain of OmpA needs to extend further from the OM, as the distance between the OM and PG increases when Lpp sits perpendicular to the OM [34]. In the absence of Lpp, OmpA determines the distance between the OM and PG [34, 35], but is not essential for cell viability [39, 40]. Taken together with the data presented here from characterization of the Lpp^{+21} phenotypes, we suggest that Lpp functions as a brace to keep the OM away from the PG layer.

The genetic screen showed that each one of the OM-located PG-binding factors Pal, YiaD and OmpA are essential (as is TolC) for viability of the Lpp^{+21} strain of *E. coli*. This is consistent with the proposition that Lpp functions to brace against the PG layer and that, in the perpendicular state, the force exerted by Lpp^{+21} would be greater than Lpp. However, the over-lap in the distance constraints measured for cells expressing Lpp and Lpp^{+21} suggests that much of the Lpp^{+21} is in the highly tilted (70±5°) form observed in the MD simulations. The enforced tilt in Lpp^{+21} means its bracing force is diminished, with the measurable

consequence that membrane integrity (SDS resistance) is diminished, OmpA and other tethers become essential to viability and the OM is highly permissive to OMV formation. Furthermore, the discovery of YiaD in the genetic screen for essential factors is significant. Previously, YiaD was suggested to be a factor regulating OMP biosynthesis by the BAM complex [41]. Structural analysis shows YiaD to be highly similar to the PG-binding domains of Pal and OmpA [42]. We suggest that the primary function of YiaD is to mediate OM-PG linkage, and that this indirectly impacts on OMP biogenesis.

Continued function of LPS transport (etc) in localized regions of the periplasm

The bridges needed to mediate LPS transport appear to be susceptible to disruption caused by Lpp^{+21} in *E. coli*. LptA is subject to degradation if the Lpt complex is compromised [7], with LptA-LptC and LptA-LptD interactions proposed as key quality control steps in the assembly of the Lpt complex [6]. That the Lpp^{+21} cells have enough Lpt complexes to maintain sufficient LPS in the OM is supported by our observations of the only minor increase in SDS sensitivity of the strain and observations by others of only minor changes in vancomycin sensitivity [23]. These findings are consistent with observations through electron microscopy that regions of the periplasm in Lpp^{+21} cells are maintained with OM-PG distances reflective of the wild-type condition, which would permit LPS transport to the OM.

All components of the PG biosynthesis pathways become essential to cell viability

In *E. coli*, the weave of the PG-layer is maintained in a uniform, open state through quality control mechanisms that depend on the regulators in the OM (LpoA and LpoB) being able to permeate it to contact the synthetases (MrcA and MrcB) in the IM. It has been hypothesized in this way that the OM lipoproteins may serve as a molecular ruler to modulate PG thickness, maintaining a single layer of PG equidistant from the OM layer under normal conditions [11]. The PG synthases encoded by *mrcA* and *mrcB* are redundant in the sense that *mrcA* mutant strains and *mrcB* mutant strains are each viable [43, 44, 45]. However, in the Lpp^{+21} strain both *mrcA* and *mrcB* (as well as their OM lipoprotein partners) are essential for viability, indicative of a compromised capability to build the PG-layer. Mutations designed to impact on these interactions lead to transient deposition of "high-density PG" and "multi-layered PG" through dysregulation of the synthetases [11]. The morphology of the PG-layer observed by electron microscopy is suggestive of these high-density and multi-layered PG consistent with transient or local impacts on the OM-PG distance [11]. An essential requirement was also placed on PG-layer remodeling, whereby the PG-binding factor NlpD was found to be essential in Lpp^{+21} cells: its function is in modulating the activity of the amidase AmiC [46, 47] to remodel PG strands, and AmiC was observed at increased steady-state levels in the Lpp^{+21} strain. Taken together with the increase in oligopeptide transporter subunits (OppB, OppC, OppD and OppF) in the Lpp^{+21} strain to recycle PG precursors across the IM, our results suggest a clearance of the malformed PG caused by dysregulation of the PG synthases is a crucial adaptation in the Lpp^{+21} strain.

Stiffness, load-bearing and connection of OM-PG

The concept of bacterial cell stiffness has emerged as a means to understand the physical parameters that define how readily bacteria can respond to major environmental changes [26, 48, 49]. Measurements by AFM have revealed a characteristic stiffness in Gram-negative bacterial cells that is contributed by load-bearing outer membrane and its attachment to the underlying PG layer [50]. In *E. coli*, mutants lacking Lpp, Pal or OmpA are "softer" than wild-type cells [50], and cells expressing the Lpp^{+21} isoform are also "softer" than wild-type cells [23]. That the Lpp^{+21} cells are softer, despite having an overall thicker, non-homogeneous PG structure as demonstrated here by EM, further supports the proposition that the OM is the major contributor to cell stiffness [48]. The steady-state levels of the GatABCD proteins respond to factors changing *E. coli* cell stiffness [22]. We observed an increase in GatABCD levels in the Lpp^{+21} cells.

Despite the length of Lpp seen in *E. coli* being conserved in a range of bacterial lineages, species from the genus *Geobacter* naturally express Lpp proteins of 99 or more residues, equivalent to Lpp^{+21} in length. *Geobacter* have a complicated periplasm housing "electron conduits" formed of transmembrane and periplasmic redox proteins, in order to transfer electrons to the external surface of the bacterial cell [51, 52]. That species of *Geobacter* serve as an exception to what is otherwise a strict rule about the length of Lpp, and thus the structurally-enforced distance constraint between the OM and PG layer, raises interesting questions about whether OM softness, OMV production or increased OM permeability might assist the unusual biological functions of the OM and periplasm in bacteria other than *E. coli*.

MATERIALS AND METHODS

Bacterial strains and growth conditions

E. coli BW25113 was the parental strain of all the recipient strains used in this study. JW5028, a derivative of BW25113, containing a kanamycin resistance marker in place of a pseudogene, was used as the wild-type for this study. Strains were grown in LB broth or M9 minimal media broth supplemented with 1 mM $MgSO_4$, 0.1mM $CaCl_2$, 1.12 mM thiamine and 0.2% (w/v) glucose for a defined minimal media. To osmotically stabilize the growth medium, sorbitol was supplemented to a final concentration of 0.5 M. For overnight cultures, strains were grown in LB broth overnight at 37 °C under continuous agitation. Subculturing was done by diluting the saturated culture 1:100 using new media. The cells were then grown to mid-exponential growth phase (OD_{600} = 0.5-0.6) at 37 °C under shaking. Culture media was supplemented with antibiotics for plasmid selection and maintenance or selection of mutants at the following concentrations: 100 µg/ml ampicillin, 30 µg/ml kanamycin, 34 µg/ml chloramphenicol. 15 g/l agar was added to media before autoclaving when solid media was required (Fig. S4).

Construction of Lpp^{+21} mutant

The endogenous *lpp* gene was replaced with the extended *lpp*$^{+21}$ gene previously described [17, 18] with minor modifications (Fig. S1). First the replacement was done in the donor *E. coli* Hfr Cavalli cells using the λ –red recombination system [53]. A gene block was sourced (Integrated DNA Technologies) containing extra 21 amino acid residues (three heptad repeats) inserted between codon 42 and 43 of *E. coli* Lpp. The gene block also contained 50 bp DNA flanking 5' and 3' ends of the *lpp*$^{+21}$ gene. On the 5' end, the extension was homologous to DNA sequence upstream of *lpp*, while on the 3' end, the extension was homologous to the *cat* gene. The gene block was combined with the *cat* gene by Gibson assembly, and the resulting PCR fragment was used to replace *lpp*. The new Lpp^{+21} strain was selected by plating on medium containing chloramphenicol. Chromosomal *lpp*$^{+21}$ was moved into *E. coli* BW25113 background by mating with kanamycin-resistant Keio collection strain JW5028, described above, to generate a double mutant [19, 54] (Fig. S4). The mutation was verified by PCR described below (Fig. S1) and sequencing.

SDS-PAGE and immunoblotting

Protein extracts were prepared from cells grown in M9 minimal media (0.5 M sorbitol), separated in 15% acrylamide gels and transferred to 0.45 µm hydrophobic Immobilon-P PVDF membrane (Merck Millipore). Immunoblotting was as described previously [19]. Rabbit primary antibodies; α-Lpp antibody (kindly provided by T. Silhavy) and α-OmpA were diluted 1:400,000 and 1: 30,000, respectively in 5% skim milk, TBST. The membranes were incubated with goat, α-rabbit IgG, HRP-conjugated secondary antibody (Sigma; 1: 20,000 in 5% skim milk, TBST), and washed with TBST. Detection was by enhanced chemiluminescence with ECL

prime western blotting detection reagent (GE Healthcare Life Sciences), visualized using Super RX-N film (Fujifilm).

Outer membrane vesicle purification and quantification

Overnight cultured cells, grown in LB without antibiotics, were washed twice in 1 x M9 salts then subcultured in 500 ml M9 minimal media supplemented with 0.5 M sorbitol (1:1000 dilution). The strains were grown to late logarithmic phase without antibiotics, $OD_{600} \approx 0.9$ and spun down to collect culture supernatant. Collected culture supernatant were then processed for OMVs isolation and purification using differential ultracentrifugation technique as discussed previously [55]. OMVs were washed twice in PBS to remove sorbitol then quantified using a bicinchoninic acid assay kit (Thermo Scientific CST#23225).

SDS sensitivity

Streaks were made on LB (solid) media with 0% SDS – 5% SDS. After 16 hrs of incubation at 37 °C, the minimum SDS concentration inhibiting growth was obtained by analyzing growth on each concentration. The streaks were done in duplicate and repeated three times.

Proteomics

Saturated overnight cultures were washed twice in 1 x M9 salts and diluted 1:100 in 10 ml M9 minimal media supplemented with 0.5 M sorbitol. Cultures were further grown to logarithmic phase, collected by centrifugation and washed using PBS buffer. The cell pellet was homogenised in 4 % SDS, 100 mM Tris, pH 8.1 and boiled at 95 °C for 10 minutes. The lysate was then sonicated with a Bioruptor® Pico (Diagenode) and protein concentration was determined with Bicinchoninic Acid assay (BCA, Thermo Fisher). SDS was removed with chloroform/methanol, the protein was digested by trypsin overnight and the digested peptides were purified with ZipTips (Agilent). Using a Dionex UltiMate 3000 RSLCnano system equipped with a Dionex UltiMate 3000 RS autosampler, an Acclaim PepMap RSLC analytical column (75 µm x 50 cm, nanoViper, C18, 2 µm, 100Å; Thermo Scientific) and an Acclaim PepMap 100 trap column (100 µm x 2 cm, nanoViper, C18, 5 µm, 100Å; Thermo Scientific), the tryptic peptides were separated by increasing concentrations of 80% ACN / 0.1% formic acid at a flow of 250 nl/min for 120 min and analyzed with a QExactive Plus mass spectrometer (Thermo Scientific). The instrument was operated in the data dependent acquisition mode to automatically switch between full scan MS and MS/MS acquisition. Each survey full scan (m/z 375–1575) was acquired in the Orbitrap with 60,000 resolution (at m/z 200) after accumulation of ions to a 3×10^6 target value with maximum injection time of 54 ms. Dynamic exclusion was set to 30 seconds. The 20 most intense multiply charged ions ($z \geq 2$) were sequentially isolated and fragmented in the collision cell by higher-energy collisional dissociation (HCD) with a fixed injection time of 54 ms, 15,000 resolution and automatic gain control (AGC) target of 2×10^5.

The raw data files were analyzed using MaxQuant software suite v1.6.5.0 [56] against Andromeda search engine [57] for protein identification and to obtain their respective label-free quantification (LFQ) values using in-house standard parameters. The proteomics data was analyzed using LFQ-Analyst [58] and the analysis of the data quality analysis is presented in Fig S6. Due to the 21 amino acid insertion in the Lpp^{+21} isoform, the relative levels of Lpp in the mutant had to be assessed manually. Only the unique peptide (IDQLSSDVQTLNAK) shared between the two isoforms was used to quantify the levels of Lpp and Lpp^{+21} in the wild-type and mutant strain, respectively (Fig S2).

To estimate the total relative amount of proteins from the various subcellular compartments, the raw intensities from peptides identified from proteins from different subcellular locations were summed and divided by the total summed intensity from all peptides. Sub-cellular locations annotations were applied from the STEPdb 2.0 [25] where proteins designated F1, A, R, and N were classified as cytoplasmic; B was designated inner membrane; H, X, and F4 were designated outer membrane / extracellular; and I, G F2, F3, and E were designated as periplasmic.

Sequence similarity network analysis

Proteobacterial proteins containing the Pfam domain (PF00691) were extracted from the Representative Proteome 35% co-membership rpg-35 group [59] and a sequence similarity network was generated with the EFI Enzyme Similarity Tool [60]. This network was visualized with Cytoscape [61] with a similarity score cutoff of 30. Each protein is represented by a colored circle node and each similarity match above the similarity score cutoff is represented by an edge between nodes with the length determined by the similarity score.

Lpp length distribution across bacterial species

To determine the amino acid length distribution of Lpp in Gammaproteobacteria (Table S4), amino acid sequences were sourced from the InterPRO database (version 81.0) [62] using the Interpro Family tag - Murein-lipoprotein (IPR016367). Filtered Lpp sequences were then concatenated into representative nodes (at least >90% sequence similarity) using the online available amino acid Initiative-Enzyme Similarity Tool (EFI-EST) [60].

Synthetic genetic interaction array

The Lpp^{+21} isoform was transferred to each of the Keio collection clones by conjugation as described (Fig. S4). First, the Hfr chloramphenicol resistant Lpp^{+21} strain was arrayed in 384-colony density on LB agar containing chloramphenicol using the Singer rotor HAD (Singer Instruments, United Kingdom). Similarly, the Keio collection arrayed in 384-colony density was pinned on LB agar plates containing kanamycin and incubated overnight at 37 °C. Using the Singer rotor HDA, the Hfr Lpp^{+21} strain and the Keio collection clones from the 384-colony density were then co-pinned onto LB agar plates and incubated at 37 °C for 16 hours.

Following conjugation, the colonies were transferred to LB agar with kanamycin (selection 1) at the same colony density and incubated at 37 °C for 16 hours. To select for double mutants (selection 2), colonies from the intermediate selection were pinned on LB agar with both kanamycin and chloramphenicol and incubated at 37 °C for 14 hours. For assessment of synthetic genetic interaction in nutrient-limited media, the double mutants generated were replica pinned in M9 minimal media at the same density and incubated at 37 °C for 25-30 hours. Images were acquired using Phenobooth (Singer Instruments, United Kingdom) for analysis. Images were manually screened to cross-reference recipient plate images to the final double antibiotic selection plates images. Candidate synthetic lethal or growth-compromised mutants were then subjected to another round of screening in the same conditions as previously identified (mini-screen) for validation. Four biological replicates were included that were further arrayed in four technical replicates.

Since the Keio collection *yiaD* mutant has been identified as containing a potential duplication event [63], the candidate *yiaD* synthetic lethal interaction was confirmed through independently constructing a *yiaD* mutant in the BW25113 strain background (Fig. S5). The lpp^{+21} variant was subsequently generated in this mutant as described above. As with the Keio *yiaD* mutant, this strain demonstrated synthetic lethality on M9 media.

Two colony PCR reactions [53, 63] (Fig. S4) confirmed the identity of all candidate double mutants, using a set of primers flanking the *lpp* gene, and a set of primers flanking the kanamycin gene (Table S5).

Preparation of Electron Cryo-microscopy samples, data collection and analysis

Strains were grown aerobically in M9 minimal media (0.5 M sorbitol) until an OD_{600} of 0.6 was reached. Cells were collected by spinning at 6000xg for 5 minutes and resuspended to an OD_{600} of ≈ 12. Cryo-EM, data collection and analysis were performed as described previously [17, 18].

Generation of simulation systems

Initially, two systems were generated: the OM and PG, as previously detailed [49], with two copies of wild-type Lpp and with two copies of Lpp^{+21}. For wild-type Lpp, we used the homo trimer from PDB 1EQ7 [33]. For Lpp^{+21}, a monomer was first built using I-TASSER [64]. Next, the trimer of Lpp^{+21} was built using the wild-type Lpp trimer as a template, further optimized using Targeted Molecular Dynamics (TMD) for 1 ns. For both Lpp and Lpp^{+21}, the proteins were anchored in the OM via N-terminal acylation while the C-terminus of one copy from each trimer was covalently linked to the PG. The systems generated were prepared for equilibration using the following steps for 1 ns each: 1) minimization for 10,000 steps, 2) melting of lipid tails, 3) restraining only the PG and the protein, and 4) restraining the PG and the protein backbone. Both systems were equilibrated for 200 ns.

For each of the two systems (Lpp and Lpp^{+21}), a new system was constructed with one Lpp trimer removed and OmpA inserted into the OM. The full-length OmpA structure was taken from Ortiz-Suarez *et al.* [65]. The

473 periplasmic domain region of the OmpA (clamp, hereafter) was lowered to the PG by shortening the distance
474 between the PG and the clamp for 20 ns. After the clamp was lowered, it was clenched to the nearest DAP
475 residue by using two different distance collective variables [66] between the centre of mass of residue 242 or
476 256 from OmpA and that of a nearby PG DAP residue to maintain the connection for 110 ns. In the case of
477 Lpp^{+21}, PG was first pulled towards the OM to match the distance between them in wild-type Lpp, after which
478 the clamp of OmpA was lowered and clenched for 110 ns. The wild-type Lpp/OmpA system was equilibrated
479 for 200 ns; OmpA stayed bound to the PG without colvars. The Lpp^{+21}/OmpA system was also equilibrated
480 for 200 ns, but colvars were needed to maintain the OmpA-PG interaction.
481
482 ***Molecular Dynamics (MD)***
483 All-atom molecular dynamics simulations were performed using NAMD 2.11 [67] and the CHARMM36m [68]
484 and CHARMM36 [69] force-field parameters for proteins and lipids, respectively, with the TIP3P-CHARMM
485 water model [70]. Unless otherwise stated, all MD simulations were performed under a periodic boundary
486 condition with a cut-off at 12 Å for short-range electrostatic and Lennard-Jones interactions with a force-based
487 switching function starting at 10 Å. For long range electrostatic calculations, the particle-mesh Ewald method
488 [71] with a grid spacing of at most 1 Å was used for long-range electrostatic calculations. Bonds between a heavy
489 atom and a hydrogen atom were maintained to be rigid, while all other bonds remain flexible. Unless otherwise
490 stated, each system was equilibrated under an isothermal-isobaric ensemble (NPT) at 310 K and 1 bar, with a
491 timestep of 4 fs after hydrogen mass repartitioning [72]. A Langevin thermostat with a damping coefficient of 1
492 ps^{-1} was used for temperature control and a Langevin piston was used for pressure control. VMD was used for
493 all visualization and analysis [73].
494

ACKNOWLEDGEMENTS

We are grateful to Rebecca Bamert and Jonathan Wilksch for critical comments on the manuscript. The authors thank Andrea Nans and Peter Rosenthal at the Francis Crick Institute for electron microscopy services, and support staff at the Monash Proteomic & Metabolomic Facility. We acknowledge research support from the Australian Research Council (FL130100038 to T.L. and I.D.H.). E.M. was recipient of a Monash Research Scholarship.

FIGURE LEGENDS

Figure 1. **Phenotypes of *E. coli* cells encoding the Lpp^{+21} isoform.** (A) Non-redundant Lpp sequences were identified (Methods) and the protein length charted on the x-axis. The number of non-redundant sequences showing that length is shown on the y-axis. The location of Lpp and the lengthened Lpp^{+21} are indicated. (B) Whole cell lysates were prepared from the indicated strains and subject to SDS-PAGE and immunoblot analysis with anti-Lpp antibodies and anti-OmpA antibodies. OmpA serves as a loading control. (C) The JW5028 – Keio BW25113 strain with *kan* gene replacing a pseudogene background and isogenic Lpp^{+21} strain (Fig. S1) were grown over 24 hours. The growth medium is M9, containing the indicated concentration of sorbitol as an osmolyte. (D) Growth rates for the same strains were measured in rich (LB) growth media with and without sorbitol over 20 hours. (E) The periplasmic width distribution of the indicated strains in hyperosmotic conditions. While PG layer in the wild-type strain is a uniform thin electron dense layer, the PG layer in the Lpp^{+21} strain is more diffuse and thicker. (F) Cryo EM of cell envelopes in hyperosmotic conditions. Measurements from EM views evaluate the distance between OM and PG in the Lpp^{+21} strain micrographs. The histogram depicts the frequency with which a given distance is observed between the OM and PG.

Figure 2. **The Lpp^{+21} cells have softened outer membranes and increased blebbing.** (A) Heat map of the significant proteomic differences observed between the wild-type and Lpp^{+21} mutant. Blue boxes indicate a relative reduction and red indicates a relative increase in protein level, centred on the average of the replicate samples. The grouping of the proteins is based on the similarity of the change in expression observed. (B) The Lpp^{+21} mutant has an overall reduction in the level of periplasmic proteins. (C) The Lpp^{+21} mutant has an increase in protein secreted via OMV blebbing. (D) SDS sensitivity profiles of the Lpp^{+21} mutant compared to the wild-type in increasing concentration of SDS in LB (solid) media. Representative data are shown from experiments performed in triplicate.

Figure 3. Factors that become essential to mediate OM-PG linkage in Lpp^{+21} *E. coli*. (A) The growth phenotype in M9 minimal media (0.5 M sorbitol) of single gene knock outs that exhibit essentiality on Lpp^{+21} background (Table 1). (B) The growth phenotype in M9 minimal media (0.5 M sorbitol) of double gene mutants. The mutants are results of Hfr Cavalli *lpp:lpp^{+21} cat* crossed with 22 Kan^{R} recipients shown in panel A (methods). The double mutants are indicated and are arranged in 4 biological replicates (each having 4 technical replicates). (C) Sequence similarity network of domain (Pfam PF00691) containing proteins from across the Proteobacteria. Each circle represents a protein from a representative proteome (rp35) containing the PF00691 domain, connected by lines with a length imparted by their similarity score as defined by EFI - Enzyme Similarity Tool [60], with a cutoff of 30. Proteins are colored by their taxonomic class and the approximate location of the *E. coli* K12 six PF00691 proteins is indicated. (D) Synthetic lethal phenotype of

538 the drug efflux mutants in the absence of selective antibiotics in M9 minimal media condition. Representative
539 data are shown from experiments performed in biological triplicate.
540
541 **Figure 4. Final states of the OM-PG linkage from MD simulations.** (A-B). A patch of OM with the LPS
542 molecules depicted in orange (lipid A moiety) and yellow (core oligosaccharides), and the phospholipids in
543 the inner leaflet of the OM depicted in grey. The PG layer (blue for glycans and green for peptide crosslinks)
544 is attached to the OM via two trimers of Lpp (A), or a trimer of Lpp and the PG-binding domain of OmpA
545 (red). The β-barrel anchor of OmpA is shown embedded in the OM. (C-D) Equivalent scenarios formed with
546 Lpp^{+21} trimers. The distances shown are calculated from the inner face of the OM to the centre of the PG layer
547 and represent the average over the last 100 ns of a 200-ns simulation.
548

SUPPLEMENT

Figure S1. Construction and assessment of Lpp^{+21} *E. coli*. (A) Schematic representation of the elongated Lpp^{+21} isoform. The strain was constructed by inserting (red lettering) heptad repeats between residue D42 and Q43 of Lpp. (B) Schematic detailing the isogenic replacement of the *lpp* gene with the *lpp*$^{+21}$ gene. (C) PCR confirmation of the *lpp*$^{+21}$ mutant strain (Methods).

Figure S2. Quantitation of Lpp and Lpp^{+21} isoforms. The sequence of the 21 residues inserted to create the Lpp^{+21} isoform is also indicated. Mass spectrometry data for Lpp vs Lpp^{+21} was reanalyzed after extraction from the whole cell proteomic data. Given the different tryptic peptides generated from the two isoforms of Lpp, a shared peptide (red) was used to quantify the relative levels of each Lpp isoform in each of the strains. The graphs document the relative levels of the peptide and show that the presence or absence of sorbitol in the growth medium has no effect on the level of Lpp^{+21} relative to Lpp.

Figure S3. Sub-cellular proteomics of Lpp^{+21} *E. coli*. (A) Relative amount of protein in different subcellular compartments, measured by the raw relative proportion of peptide intensities identified from proteins annotated to reside in cellular compartments defined in the STEPdb. (B) Comparative proteome profile of the wild-type and Lpp^{+21} strain for cell lysate and extracted outer membrane vesicles. Loading of each technical replicate was normalized to OD_{600}. Representative data are shown from experiments performed in biological triplicate.

Figure S4. A synthetic lethal screen to determine genes essential to Lpp^{+21} *E. coli*. An Hfr donor strain carrying a selectable marker (*cat*) fused to *lpp*$^{+21}$, replacing the *lpp* ORF, is mated on agar plates with arrayed F$^-$ recipients (384) per plate carrying a selectable marker (*kan*) replacing other ORF. Upon mating, cells are subjected the first round of selection (intermediate selection) using antibiotic kanamycin and then further subjected to a second round of selection using both antibiotics; (A) depicts images of representative plates generated in each step of the procedure with imaging and manual analysis step, cross-referencing of single gene knock outs and double recombinants, included. (B) depiction of the strains as cartoons generated in each step of the procedure. (C) A representative mini screen of manually selected genes from the main synthetic lethal screen. Sterility controls were included on each mini screen. The mini screen was performed in 384-pin density with each clone arrayed in four biological replicates, each having four technical replicates (blue boxes). Synthetic lethal mutants identified from the mini screen were further verified by PCR to confirm the presence of both gene modifications and rule out partial duplication events.

Figure S5. Construction and characterization of the validation *yiaD* mutant. A kanamycin resistance cassette was amplified from pKD4 using primers with overhangs complementary to upstream and downstream

of *yiaD.* The PCR fragment was electroporated in BW25113 cells harbouring the λ –red recombineering plasmid (pKD46). Transformants were selected on kanamycin-resistant plates and verified by PCR (methods). Primers flanking the *yiaD* gene confirm replacement of *yiaD* with kanamycin cassette and primers amplifying lpp confirm lpp^{+21} replacement of *lpp*. The sequence information for all primers used are included in Table S5.

Figure S6. Proteomics quality control report. (A) Principle Component Analysis (PCA) plot of data from triplicate samples of wild-type and Lpp^{+21} strains grown on M9 medium with or without supplementation by sorbitol. (B) Sample Coefficient of variation plots for the same four samples.

Table S1 Proteomic results

Table S2. Substantive changes in steady-state protein levels in cell envelope of Lpp^{+21}

Table S3: Proteins used in the generation of the sequence similarity network

Table S4: Representative Lpp protein information

Table S5: Bacterial strains and primers used in the study

REFERENCES

1. Silhavy TJ, Kahne D, Walker S. The bacterial cell envelope. *Cold Spring Harb Perspect Biol* **2**, a000414 (2010).

2. Gunasinghe SD*, et al.* The WD40 Protein BamB Mediates Coupling of BAM Complexes into Assembly Precincts in the Bacterial Outer Membrane. *Cell Rep* **23**, 2782-2794 (2018).

3. Rassam P*, et al.* Supramolecular assemblies underpin turnover of outer membrane proteins in bacteria. *Nature* **523**, 333-336 (2015).

4. Ursell TS, Trepagnier EH, Huang KC, Theriot JA. Analysis of surface protein expression reveals the growth pattern of the gram-negative outer membrane. *PLoS Comput Biol* **8**, e1002680 (2012).

5. Freinkman E, Okuda S, Ruiz N, Kahne D. Regulated assembly of the transenvelope protein complex required for lipopolysaccharide export. *Biochemistry* **51**, 4800-4806 (2012).

6. Sperandeo P, Martorana AM, Polissi A. The lipopolysaccharide transport (Lpt) machinery: A nonconventional transporter for lipopolysaccharide assembly at the outer membrane of Gram-negative bacteria. *J Biol Chem* **292**, 17981-17990 (2017).

7. Sperandeo P*, et al.* New insights into the Lpt machinery for lipopolysaccharide transport to the cell surface: LptA-LptC interaction and LptA stability as sensors of a properly assembled transenvelope complex. *J Bacteriol* **193**, 1042-1053 (2011).

8. Ekiert DC*, et al.* Architectures of Lipid Transport Systems for the Bacterial Outer Membrane. *Cell* **169**, 273-285 e217 (2017).

9. Shrivastava R, Chng SS. Lipid trafficking across the Gram-negative cell envelope. *J Biol Chem* **294**, 14175-14184 (2019).

10. Pazos M, Peters K, Vollmer W. Robust peptidoglycan growth by dynamic and variable multi-protein complexes. *Curr Opin Microbiol* **36**, 55-61 (2017).

11. Typas A, Banzhaf M, Gross CA, Vollmer W. From the regulation of peptidoglycan synthesis to bacterial growth and morphology. *Nat Rev Microbiol* **10**, 123-136 (2011).

12. Paradis-Bleau C*, et al.* Lipoprotein cofactors located in the outer membrane activate bacterial cell wall polymerases. *Cell* **143**, 1110-1120 (2010).

13. Typas A*, et al.* Regulation of peptidoglycan synthesis by outer-membrane proteins. *Cell* **143**, 1097-1109 (2010).

14. Selkrig J, *et al.* Conserved features in TamA enable interaction with TamB to drive the activity of the translocation and assembly module. *Sci Rep* **5**, 12905 (2015).

15. Selkrig J, *et al.* Discovery of an archetypal protein transport system in bacterial outer membranes. *Nat Struct Mol Biol* **19**, 506-510, S501 (2012).

16. Shen HH, *et al.* Reconstitution of a nanomachine driving the assembly of proteins into bacterial outer membranes. *Nat Commun* **5**, 5078 (2014).

17. Cohen EJ, Ferreira JL, Ladinsky MS, Beeby M, Hughes KT. Nanoscale-length control of the flagellar driveshaft requires hitting the tethered outer membrane. *Science* **356**, 197-200 (2017).

18. Asmar AT, *et al.* Communication across the bacterial cell envelope depends on the size of the periplasm. *PLoS Biol* **15**, e2004303 (2017).

19. Baba T, *et al.* Construction of *Escherichia coli* K-12 in-frame, single-gene knockout mutants: the Keio collection. *Mol Syst Biol* **2**, 2006 0008 (2006).

20. Stock JB, Rauch B, Roseman S. Periplasmic space in *Salmonella typhimurium* and *Escherichia coli*. *J Biol Chem* **252**, 7850-7861 (1977).

21. Ingraham JL, Marr AG. Effects of temperature, pressure, pH, and osmotic stress on growth. In: *Escherichia coli and Salmonella: cellular and molecular biology* (eds Neidhardt FC, *et al.*). ASM Press (1996).

22. Domka J, Lee J, Bansal T, Wood TK. Temporal gene-expression in *Escherichia coli* K-12 biofilms. *Environ Microbiol* **9**, 332-346 (2007).

23. Mathelie-Guinlet M, Asmar AT, Collet JF, Dufrene YF. Lipoprotein Lpp regulates the mechanical properties of the *E. coli* cell envelope. *Nat Commun* **11**, 1789 (2020).

24. Li GW, Burkhardt D, Gross C, Weissman JS. Quantifying absolute protein synthesis rates reveals principles underlying allocation of cellular resources. *Cell* **157**, 624-635 (2014).

25. Loos MS, *et al.* Structural Basis of the Subcellular Topology Landscape of *Escherichia coli*. *Front Microbiol* **10**, 1670 (2019).

26. Rojas ER, Huang KC, Theriot JA. Homeostatic Cell Growth Is Accomplished Mechanically through Membrane Tension Inhibition of Cell-Wall Synthesis. *Cell Syst* **5**, 578-590 e576 (2017).

27. Soltes GR, Martin NR, Park E, Sutterlin HA, Silhavy TJ. Distinctive Roles for Periplasmic Proteases in the Maintenance of Essential Outer Membrane Protein Assembly. *J Bacteriol* **199**, (2017).

691 28. Li H. Aligning sequence reads, clone sequences and assembly contigs with BWA-MEM. *ArXiv* **1303**,
692 (2013).

693
694 29. Xu Y*, et al.* Assembly and channel opening of outer membrane protein in tripartite drug efflux pumps
695 of Gram-negative bacteria. *J Biol Chem* **287**, 11740-11750 (2012).

696
697 30. Kim S, Yum S, Jo WS, Lee BL, Jeong MH, Ha NC. Expression and biochemical characterization of
698 the periplasmic domain of bacterial outer membrane porin TdeA. *J Microbiol Biotechnol* **18**, 845-851
699 (2008).

700
701 31. Jo I, Kim JS, Xu Y, Hyun J, Lee K, Ha NC. Recent paradigm shift in the assembly of bacterial tripartite
702 efflux pumps and the type I secretion system. *J Microbiol* **57**, 185-194 (2019).

703
704 32. Shi X*, et al.* In situ structure and assembly of the multidrug efflux pump AcrAB-TolC. *Nat Commun*
705 **10**, 2635 (2019).

706
707 33. Shu W, Liu J, Ji H, Lu M. Core structure of the outer membrane lipoprotein from *Escherichia coli* at
708 1.9 A resolution. *J Mol Biol* **299**, 1101-1112 (2000).

709
710 34. Boags AT, Samsudin F, Khalid S. Binding from Both Sides: TolR and Full-Length OmpA Bind and
711 Maintain the Local Structure of the *E. coli* Cell Wall. *Structure* **27**, 713-724 e712 (2019).

712
713 35. Samsudin F, Boags A, Piggot TJ, Khalid S. Braun's Lipoprotein Facilitates OmpA Interaction with the
714 *Escherichia coli* Cell Wall. *Biophys J* **113**, 1496-1504 (2017).

715
716 36. Asmar AT, Collet JF. Lpp, the Braun lipoprotein, turns 50-major achievements and remaining issues.
717 *FEMS Microbiol Lett* **365**, (2018).

718
719 37. Inouye M, Shaw J, Shen C. The assembly of a structural lipoprotein in the envelope of *Escherichia*
720 *coli*. *J Biol Chem* **247**, 8154-8159 (1972).

721
722 38. Miller SI, Salama NR. The gram-negative bacterial periplasm: Size matters. *PLoS Biol* **16**, e2004935
723 (2018).

724
725 39. Babu M*, et al.* Quantitative genome-wide genetic interaction screens reveal global epistatic
726 relationships of protein complexes in *Escherichia coli*. *PLoS Genet* **10**, e1004120 (2014).

727
728 40. Babu M*, et al.* Genetic interaction maps in *Escherichia coli* reveal functional crosstalk among cell
729 envelope biogenesis pathways. *PLoS Genet* **7**, e1002377 (2011).

730
731 41. Tachikawa T, Kato J. Suppression of the temperature-sensitive mutation of the *bamD* gene required
732 for the assembly of outer membrane proteins by multicopy of the yiaD gene in *Escherichia coli*. *Biosci*
733 *Biotechnol Biochem* **75**, 162-164 (2011).

42. Ishida H, Garcia-Herrero A, Vogel HJ. The periplasmic domain of *Escherichia coli* outer membrane protein A can undergo a localized temperature dependent structural transition. *Biochim Biophys Acta* **1838**, 3014-3024 (2014).

43. Cho H*, et al.* Bacterial cell wall biogenesis is mediated by SEDS and PBP polymerase families functioning semi-autonomously. *Nat Microbiol* **1**, 16172 (2016).

44. Mueller EA, Egan AJ, Breukink E, Vollmer W, Levin PA. Plasticity of *Escherichia coli* cell wall metabolism promotes fitness and antibiotic resistance across environmental conditions. *Elife* **8**, (2019).

45. Suzuki H, Nishimura Y, Hirota Y. On the process of cellular division in *Escherichia coli*: a series of mutants of *E. coli* altered in the penicillin-binding proteins. *Proc Natl Acad Sci U S A* **75**, 664-668 (1978).

46. Stohl EA, Lenz JD, Dillard JP, Seifert HS. The Gonococcal NlpD Protein Facilitates Cell Separation by Activating Peptidoglycan Cleavage by AmiC. *J Bacteriol* **198**, 615-622 (2015).

47. Yang LC, Gan YL, Yang LY, Jiang BL, Tang JL. Peptidoglycan hydrolysis mediated by the amidase AmiC and its LytM activator NlpD is critical for cell separation and virulence in the phytopathogen *Xanthomonas campestris*. *Mol Plant Pathol* **19**, 1705-1718 (2018).

48. Rojas ER, Huang KC. Regulation of microbial growth by turgor pressure. *Curr Opin Microbiol* **42**, 62-70 (2018).

49. Hwang H, Paracini N, Parks JM, Lakey JH, Gumbart JC. Distribution of mechanical stress in the *Escherichia coli* cell envelope. *Biochim Biophys Acta Biomembr* **1860**, 2566-2575 (2018).

50. Rojas ER*, et al.* The outer membrane is an essential load-bearing element in Gram-negative bacteria. *Nature* **559**, 617-621 (2018).

51. Jimenez Otero F, Chan CH, Bond DR. Identification of Different Putative Outer Membrane Electron Conduits Necessary for Fe(III) Citrate, Fe(III) Oxide, Mn(IV) Oxide, or Electrode Reduction by *Geobacter sulfurreducens*. *J Bacteriol* **200**, (2018).

52. Santos TC, Silva MA, Morgado L, Dantas JM, Salgueiro CA. Diving into the redox properties of *Geobacter sulfurreducens* cytochromes: a model for extracellular electron transfer. *Dalton Trans* **44**, 9335-9344 (2015).

53. Datsenko KA, Wanner BL. One-step inactivation of chromosomal genes in *Escherichia coli* K-12 using PCR products. *Proc Natl Acad Sci U S A* **97**, 6640-6645 (2000).

54. Gagarinova A, Babu M, Greenblatt J, Emili A. Mapping bacterial functional networks and pathways in *Escherichia Coli* using synthetic genetic arrays. *J Vis Exp*, (2012).

55. Deo P, *et al.* Outer membrane vesicles from *Neisseria gonorrhoeae* target PorB to mitochondria and induce apoptosis. *PLoS Pathog* **14**, e1006945 (2018).

56. Cox J, Mann M. MaxQuant enables high peptide identification rates, individualized p.p.b.-range mass accuracies and proteome-wide protein quantification. *Nat Biotechnol* **26**, 1367-1372 (2008).

57. Cox J, Neuhauser N, Michalski A, Scheltema RA, Olsen JV, Mann M. Andromeda: a peptide search engine integrated into the MaxQuant environment. *J Proteome Res* **10**, 1794-1805 (2011).

58. Shah AD, Goode RJA, Huang C, Powell DR, Schittenhelm RB. LFQ-Analyst: An Easy-To-Use Interactive Web Platform To Analyze and Visualize Label-Free Proteomics Data Preprocessed with MaxQuant. *J Proteome Res* **19**, 204-211 (2020).

59. Chen C, *et al.* Representative proteomes: a stable, scalable and unbiased proteome set for sequence analysis and functional annotation. *PLoS One* **6**, e18910 (2011).

60. Gerlt JA, *et al.* Enzyme Function Initiative-Enzyme Similarity Tool (EFI-EST): A web tool for generating protein sequence similarity networks. *Biochim Biophys Acta* **1854**, 1019-1037 (2015).

61. Shannon P, *et al.* Cytoscape: a software environment for integrated models of biomolecular interaction networks. *Genome Res* **13**, 2498-2504 (2003).

62. Mitchell AL, *et al.* InterPro in 2019: improving coverage, classification and access to protein sequence annotations. *Nucleic Acids Res* **47**, D351-D360 (2019).

63. Yamamoto N, *et al.* Update on the Keio collection of *Escherichia coli* single-gene deletion mutants. *Mol Syst Biol* **5**, 335 (2009).

64. Yang J, Zhang Y. I-TASSER server: new development for protein structure and function predictions. *Nucleic Acids Res* **43**, W174-W181 (2015).

65. Ortiz-Suarez ML, Samsudin F, Piggot TJ, Bond PJ, Khalid S. Full-Length OmpA: Structure, Function, and Membrane Interactions Predicted by Molecular Dynamics Simulations. *Biophys J* **111**, 1692-1702 (2016).

66. Fiorin G, Klein ML, Hénin J. Using collective variables to drive molecular dynamics simulations. *Mol Phys* **111**, 3345-3362 (2013).

67. Phillips JC, *et al.* Scalable molecular dynamics with NAMD. *J Comput Chem* **26**, 1781-1802 (2005).

68. Huang J, *et al.* CHARMM36m: an improved force field for folded and intrinsically disordered proteins. *Nat Methods* **14**, 71-73 (2017).

69. Klauda JB*, et al.* Update of the CHARMM all-atom additive force field for lipids: validation on six lipid types. *J Phys Chem B* **114**, 7830-7843 (2010).

70. Jorgensen WL, Chandrasekhar J, Madura JD, Impey RW, Klein ML. Comparison of simple potential functions for simulating liquid water. *J Chem Phys* **79**, 926-935 (1983).

71. Darden TA, York DM, Pedersen LG. Particle mesh Ewald: An N log N method for Ewald sums in large systems. *J Comput Phys* **98**, 10089-10092 (1993).

72. Balusek C*, et al.* Accelerating Membrane Simulations with Hydrogen Mass Repartitioning. *J Chem Theory Comput* **15**, 4673-4686 (2019).

73. Humphrey W, Dalke A, Schulten K. VMD – Visual Molecular Dynamics. *J Mol Graphics* **14**, 33-38 (1996).

SUPPLEMENT

Attempted enlargement of the periplasmic space dictates adaptations in outer membrane plasticity and linkage to the underlying peptidoglycan layer.

Eric Mandela[1,+], Christopher J. Stubenrauch[1,+], David Ryoo[2], Hyea Hwang[3,#], Eli J. Cohen[4], Von L. Torres[1], Pankaj Deo[1], Chaille T. Webb[1], Cheng Huang[5], Ralf B. Schittenhelm[5], Morgan Beeby[4], JC Gumbart[6,*], Trevor Lithgow[1,*] & Iain D. Hay[7,*]

Figure S1. Construction and assessment of Lpp^{+21} *E. coli.* (A) Schematic representation of the elongated Lpp^{+21} isoform. The strain was constructed by inserting (red lettering) heptad repeats between residue D42 and Q43 of Lpp. (B) Schematic detailing the isogenic replacement of the *lpp* gene with the *lpp*$^{+21}$ gene. (C) PCR confirmation of the *lpp*$^{+21}$ mutant strain (Methods).

Figure S2. Quantitation of Lpp and Lpp^{+21} isoforms. The sequence of the 21 residues inserted to create the Lpp^{+21} isoform is also indicated. Mass spectrometry data for Lpp vs Lpp^{+21} was reanalyzed after extraction from the whole cell proteomic data. Given the different tryptic peptides generated from the two isoforms of Lpp, a shared peptide (red) was used to quantify the relative levels of each Lpp isoform in each of the strains. The graphs document the relative levels of the peptide and show that the presence or absence of sorbitol in the growth medium has no effect on the level of Lpp^{+21} relative to Lpp.

Figure S3. Sub-cellular proteomics of Lpp^{+21} *E. coli.* (A) Relative amount of protein in different subcellular compartments, measured by the raw relative proportion of peptide intensities identified from proteins annotated to reside in cellular compartments defined in the STEPdb. (B) Comparative proteome profile of the wild-type and Lpp^{+21} strain for cell lysate and extracted outer membrane vesicles. Loading of each technical replicate was normalized to OD $_{600}$. Representative data are shown from experiments performed in biological triplicate.

Figure S4. A synthetic lethal screen to determine genes essential to Lpp^{+21} *E. coli.* An Hfr donor strain carrying a selectable marker (*cat*) fused to *lpp*$^{+21}$, replacing the *lpp* ORF, is mated on agar plates with arrayed F$^-$ recipients (384) per plate carrying a selectable marker (*kan*) replacing other ORF. Upon mating, cells are subjected the first round of selection (intermediate selection) using antibiotic kanamycin and then further subjected to a second round of selection using both antibiotics; (A) depicts images of representative plates generated in each step of the procedure with imaging and manual analysis step, cross-referencing of single gene knock outs and double recombinants, included. (B) depiction of the strains as cartoons generated in each step of the procedure. (C) A representative mini screen of manually selected genes from the main synthetic lethal screen. Sterility controls were included on each mini screen. The mini screen was performed in 384-pin density with each clone arrayed in four biological replicates, each having four technical replicates (blue boxes). Synthetic lethal mutants identified from the mini screen were further verified by PCR to confirm the presence of both gene modifications and rule out partial duplication events.

Figure S5. Construction and characterization of the validation *yiaD* mutant. A kanamycin resistance cassette was amplified from pKD4 using primers with overhangs complementary to upstream and downstream of *yiaD.* The PCR fragment was electroporated in BW25113 cells harbouring the λ –red recombineering plasmid (pKD46). Transformants were selected on kanamycin-resistant plates and verified by PCR (methods). Primers flanking the *yiaD* gene confirm replacement of *yiaD* with kanamycin cassette and primers amplifying lpp confirm lpp^{+21} replacement of *lpp*. The sequence information for all primers used are included in Table S5.

Figure S6. Proteomics quality control report. (A) Principle Component Analysis (PCA) plot of data from triplicate samples of wild-type (WT) and Lpp+21 strains grown on M9 medium with or without supplementation by sorbitol. (B) Sample Coefficient of variation plots for the same four samples.

Table S1 Proteomic results

Table S2. Substantive changes in steady-state protein levels in cell envelope of Lpp^{+21}

Table S3: Proteins used in the generation of the sequence similarity network

Table S4: Representative Lpp protein information

Table S5: Bacterial strains and primers used in the study

A

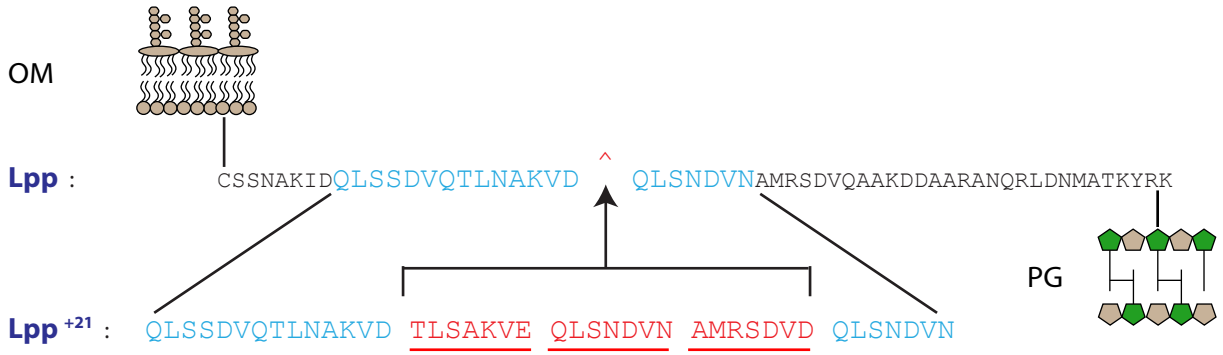

B

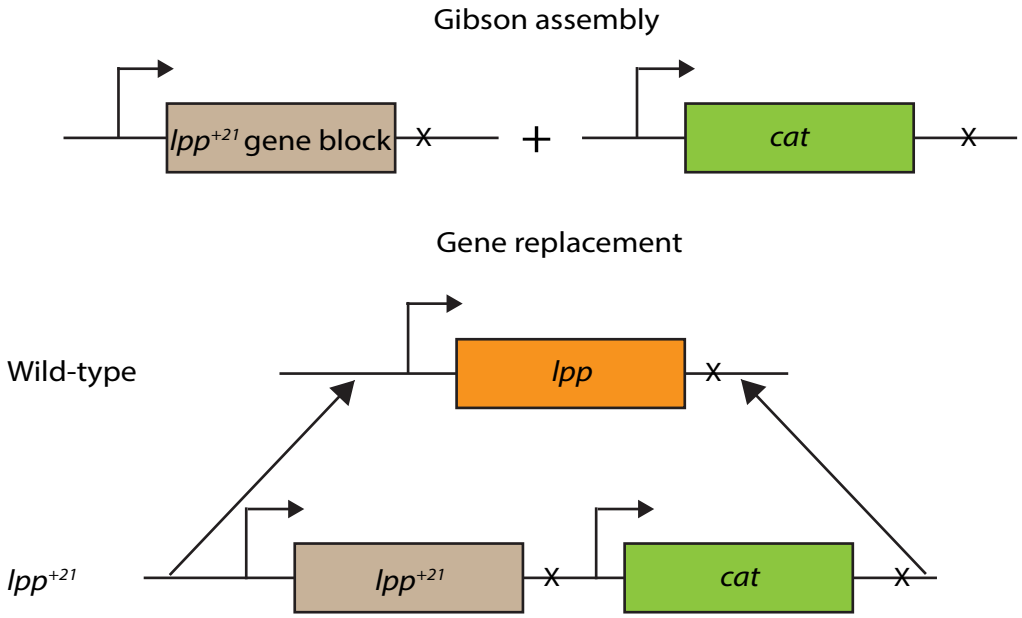

C

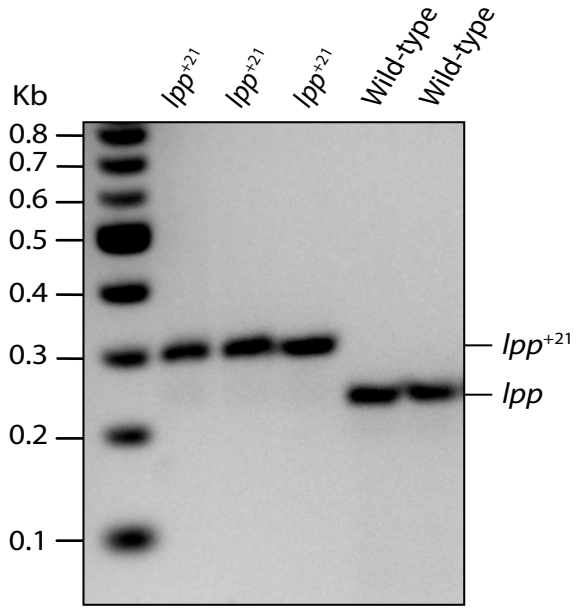

Figure S1

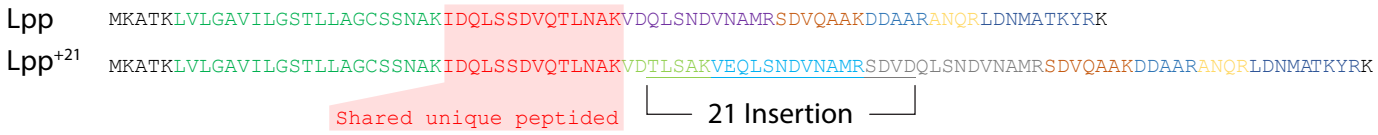

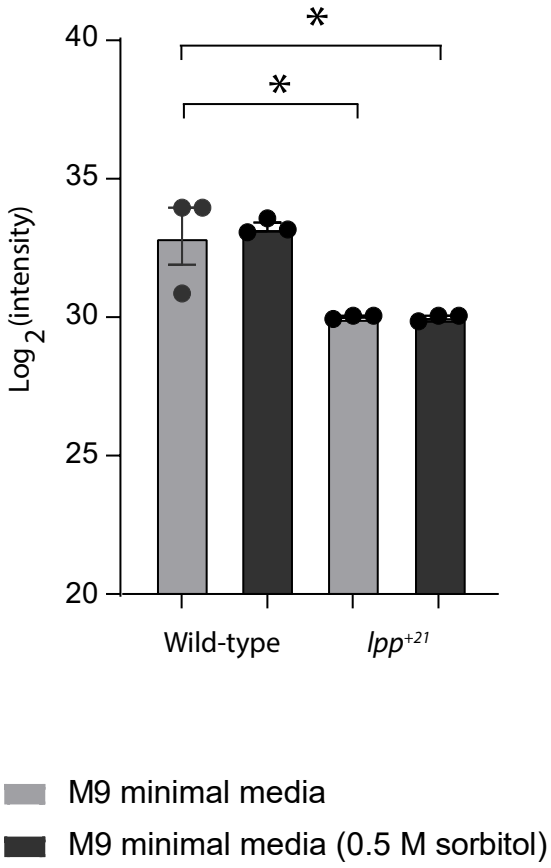

Figure S2

A

Cytoplasmic (A,N,r,F1)

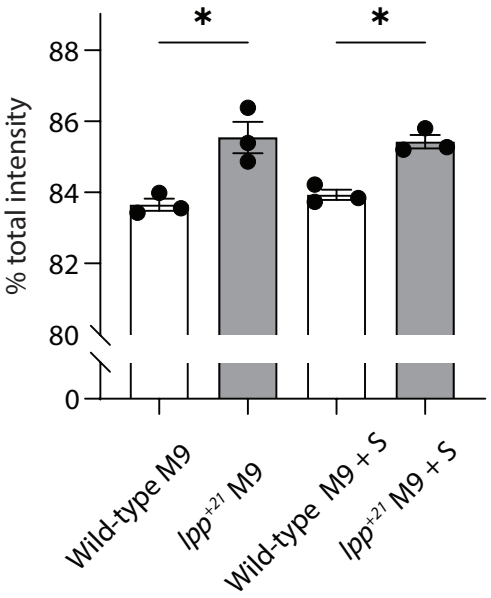

IM (B)

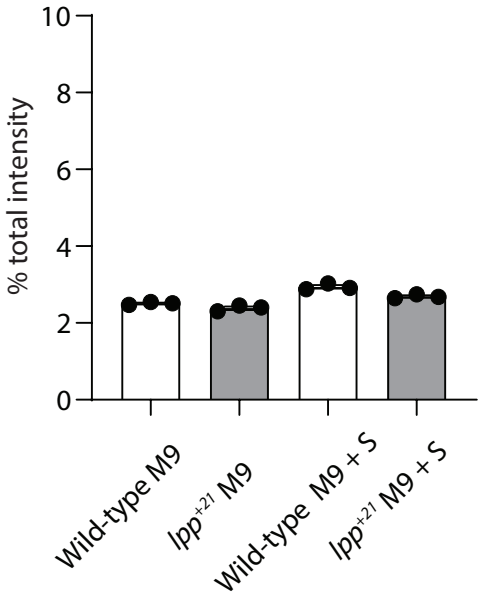

Periplasmic (G,E,F2,F3,I)

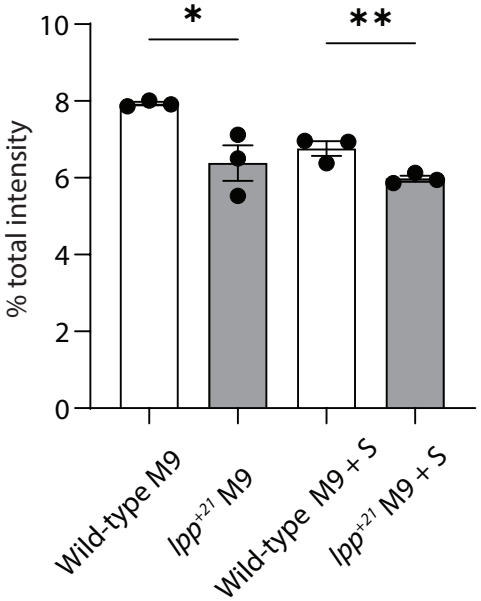

OM (H,X,F4)

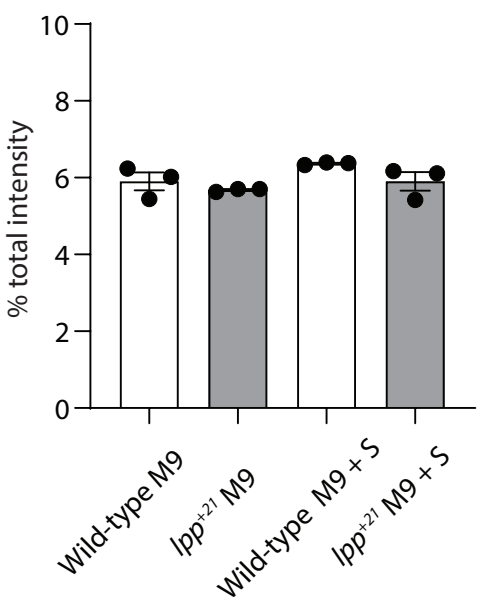

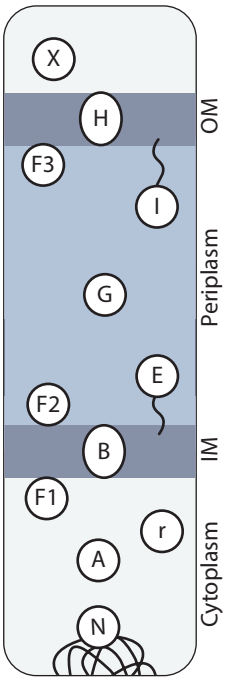

STEPdb
Sub-cellular location

B

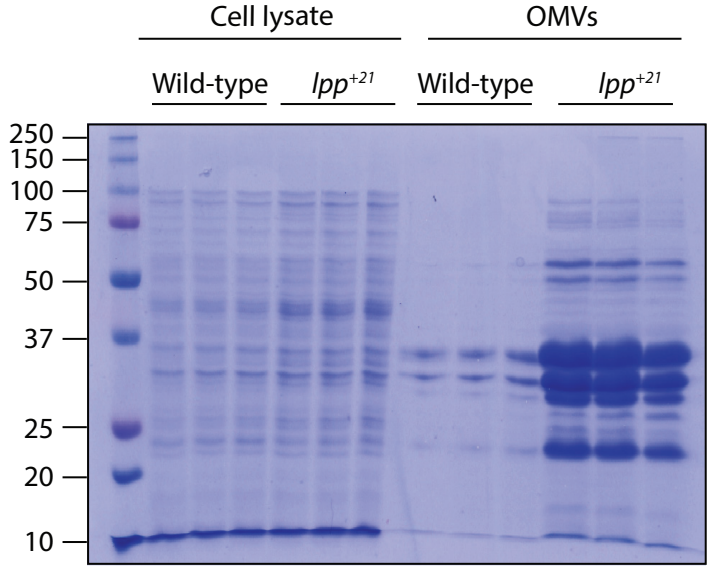

Figure S3

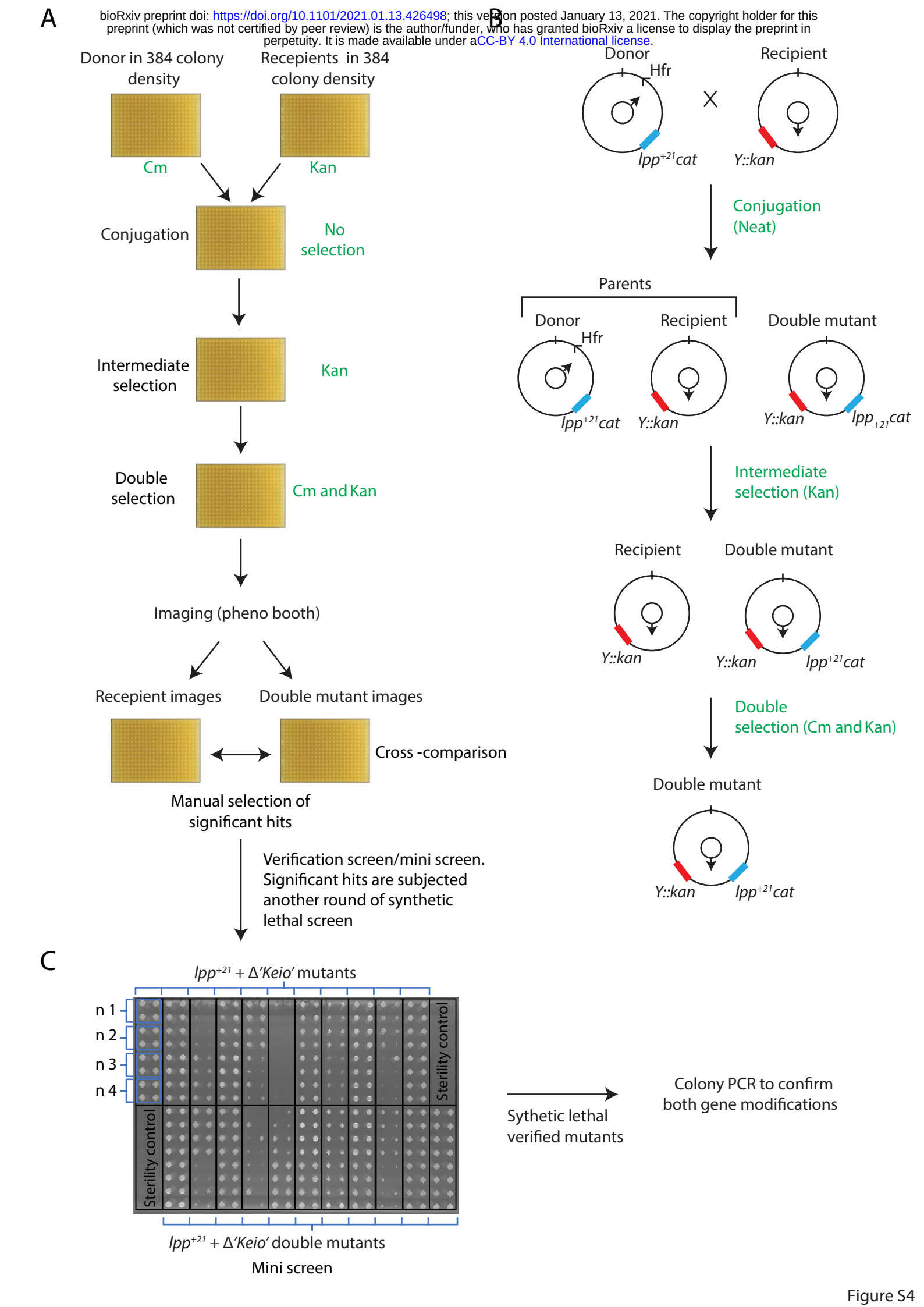

Figure S4

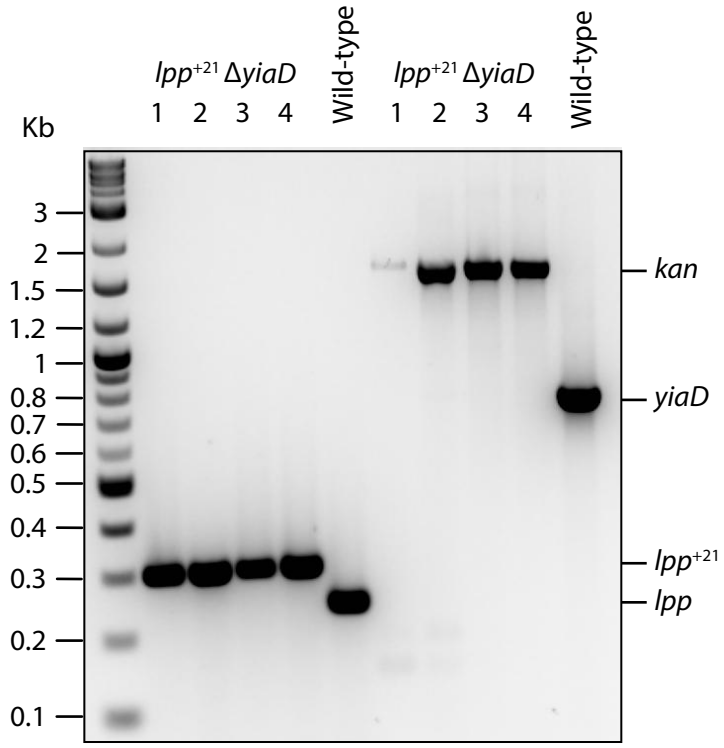

Figure S5

A

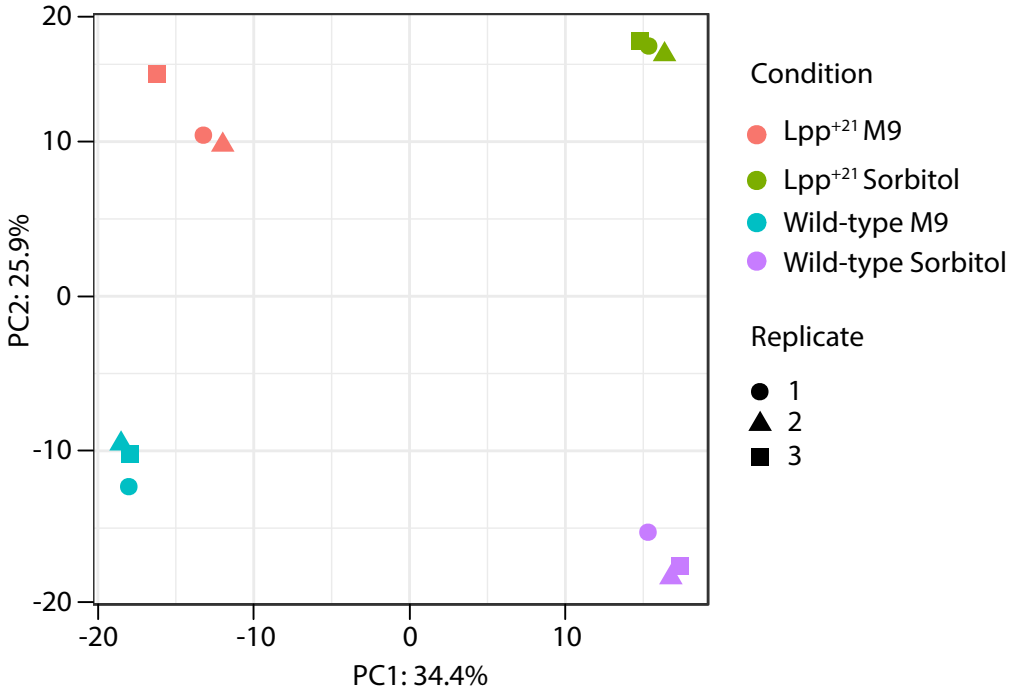

B

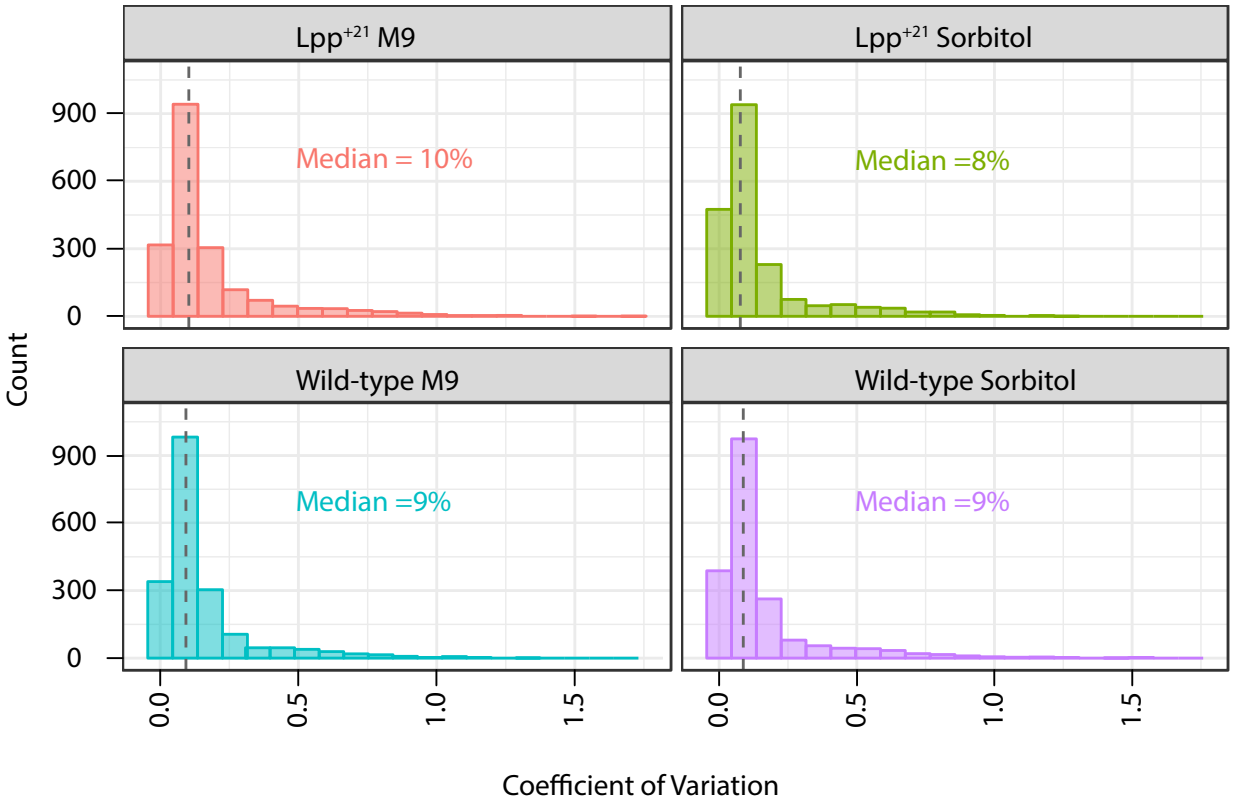

Figure S6